CAAI Transactions on Intelligence Technology

WILEY

The Institution of Engineering and Technology

ORIGINAL RESEARCH OPEN ACCESS

Fault-Tolerant Fuzzy Boundary Control for Nonlinear Distributed Parameter Systems Under Limited Measurements and Markovian Failures

Yanlin Li[1] | Kaibo Shi[1] | Yue Yu[1] | Xiangkun Wang[1] | Ming Zhu[1] | Xiao Cai[2]

[1]School of Electronic Information and Electrical Engineering, The International Joint Research Center for Perception and Control of Intelligent Rehabilitation Systems of Sichuan Province, Chengdu University, Chengdu, China | [2]Cyberspace Institute of Advanced Technology, Guangzhou University, Guangzhou, China

Correspondence: Kaibo Shi (shikaibo@cdu.edu.cn) | Xiao Cai (caixiao@gzhu.edu.cn)

Received: 24 September 2025 | **Revised:** 24 December 2025 | **Accepted:** 23 March 2026

Keywords: adaptive event-triggered mechanism | distributed parameter systems | hybrid attack | Lyapunov-Krasovskii functionals | Takagi-Sugeno fuzzy

ABSTRACT

This paper proposes a boundary control method for nonlinear distributed parameter systems (DPSs) with limited boundary measurements (BMs), as typically encountered in networked cyber-physical processes with spatially distributed dynamics such as thermal and biomedical diffusion systems. The method aims to address cyber-physical threats and hybrid attacks whilst improving state estimation accuracy and system performance. First, a partial differential equation (PDE)-based state observer is established, with an embedded adaptive event-triggered mechanism (AMET) that optimises communication through dynamic sampling adjustment. Second, a Takagi–Sugeno (T–S) fuzzy noncollocated boundary sampled-data controller (NBSDC) is designed. It adopts a spatially separated architecture to mitigate observation-actuation mismatch under partial observability. Furthermore, the controller is designed to handle hybrid attacks with inconsistent modes, including denial-of-service (DoS) interruptions and deceptive signal alterations. Their impacts are bounded by energy constraints to ensure practical feasibility. In addition, a Markov jump process is employed to characterise stochastic controller failures, capturing abrupt mode transitions and enhancing fault tolerance under adverse conditions. Third, stability analysis based on Lyapunov–Krasovskii functionals (LKFs) provides theoretical guarantees for system stability and estimation error convergence. Finally, the effectiveness and applicability of the proposed method are validated through simulations on a tumour cell diffusion model.

1 | Introduction

In recent years, parabolic partial differential equation (PDE) systems have become a widely used tool for modelling spatiotemporal dynamics across many fields, including heat conduction, reaction-diffusion transport and thermal regulation in aerospace structures [1–3]. Recent progress has been made in stabilising and controlling parabolic PDE-ODE coupled systems, in PDE-based observation/control with distributed delays and in fault-tolerant reconfiguration-oriented control for engineering platforms [4–6]. Owing to their infinite-dimensional nature, distributed parameter systems (DPSs) remain challenging for stability analysis and controller synthesis [4, 5]. These challenges are further intensified by practical factors, such as time delays and distributed-delay effects [5], input delays with event-triggered implementations [7], degradation-induced fault evolution and reliability issues [8] and quantisation/triggering constraints under uncertainties [9]. Accordingly, various analytical tools have been developed, including Lyapunov-based methods, semigroup theory and backstepping techniques, for boundary control of DPSs [10, 11].

This is an open access article under the terms of the Creative Commons Attribution-NonCommercial License, which permits use, distribution and reproduction in any medium, provided the original work is properly cited and is not used for commercial purposes.

© 2026 The Author(s). *CAAI Transactions on Intelligence Technology* published by John Wiley & Sons Ltd on behalf of The Institution of Engineering and Technology and Chongqing University of Technology.

However, limited efforts have been made to apply the T–S fuzzy modelling approach to the boundary observer design of nonlinear time-delay parabolic PDEs, which restricts the capability to handle system uncertainties and nonlinear behaviours. To overcome this limitation, fuzzy logic control has been increasingly adopted in recent years to enhance modelling accuracy and control performance for complex PDEs.

Building on these developments, the T–S fuzzy modelling framework has emerged as a powerful analytical and control tool for uncertain nonlinear systems [12–16]. By decomposing complex nonlinear systems into a set of local linear subsystems via fuzzy rules, the T–S approach enables a smooth integration of linear control theory with nonlinear reasoning. This methodology has been extended to DPSs, facilitating the design of boundary control and output feedback schemes [17, 18], and significant progress has been made in sampled-data fuzzy control (SDFC) of parabolic PDEs [19, 20]. For instance, a fuzzy boundary SDFC method for nonlinear parabolic DPSs was proposed [17]; Wang et al. [18] addressed fuzzy boundary SDFC for DPSs with random time-varying delays. The observer-based H_∞ SDFC method for nonlinear parabolic PDEs was studied [19], whereas a spatially varying gain SDFC strategy was developed for time-delay parabolic PDEs [20].

Nonetheless, most fuzzy observer designs rely on periodic communication and ideal network conditions, which are often infeasible in real-world applications. To alleviate communication burden, event-triggered sampled-data (ETSD) strategies have been proposed, which update control or observation signals only when necessary. These strategies have shown promising results in both ordinary differential equation (ODE) and PDEs [21, 22]. However, most existing methods still assume full-state measurements or spatially collocated hardware and pay limited attention to practical threats.

With the increasing openness of networked control systems, cybersecurity threats, such as DoS, deception and replay attacks, pose serious risks to system operation [23–27]. At the same time, actuator faults caused by ageing or external disturbances further degrade system reliability. For instance, evaluating control accuracy under DoS disturbances in dual-path networked control frameworks was investigated [25], whereas asymptotic stability of NCSs under DoS attacks with bandwidth constraints was studied [26]. Wang et al. [27] proposed a fault-tolerant ETSD fuzzy control approach for nonlinear time-delay parabolic PDEs under spatially pointwise measurement constraints. However, these studies mostly focus on specific network attack scenarios, with insufficient attention to actuator or sensor faults common in engineering practice.

In real-world systems, actuators are often subject to environmental disturbances, mechanical wear or ageing, which can lead to failure and significantly affect system safety and stability. To address this, several fault-tolerant control schemes have been proposed to improve robustness against actuator anomalies [28–31]. Nevertheless, most of these works treat actuator faults or cyber-attacks in isolation, without fully considering their combined effects. Fortunately, recent studies have begun to explore secure control of nonlinear ODE systems subject to both cyber-attacks and actuator faults [32, 33]. In addition, an ETSD fuzzy secure control method for nonlinear parabolic PDEs under random actuator failures and deception attacks was investigated [34]. A noncollocated output feedback approach for reaction-diffusion systems under intermittent BMs is investigated [35]. Although some progress has been made, there is still a shortage of fuzzy sampled-data controller designs that can simultaneously cope with hybrid cyber-attacks and random actuator faults, especially for nonlinear parabolic DPSs with noncollocated BMs.

To bridge this gap, the present work integrates a Takagi–Sugeno fuzzy boundary observer, an adaptive ETSD mechanism and a fault-tolerant boundary controller into a unified framework that explicitly models hybrid cyber-attacks and Markovian actuator failures for nonlinear parabolic DPSs with noncollocated BMs, thereby providing a new fuzzy sampled-data design paradigm for secure control of distributed processes and motivating the current study.

The following three aspects constitute the major contributions of this research:

1. An improved boundary sampled-data observer is proposed based on the PDE modelling framework, incorporating an AETM to dynamically adjust the sampling interval. Under BMs conditions, this approach effectively reduces communication overhead whilst maintaining high estimation accuracy.
2. A T–S fuzzy NBSDC with a spatially separated architecture is proposed to address observation–actuation asymmetry. The design mitigates performance degradation caused by partial observability and improves closed-loop stability in networked control environments.
3. The proposed controller integrates a hybrid attack modelling mechanism that captures inconsistent behaviours such as denial-of-service interruptions and deceptive signal injections. The activation is governed by a random process, and energy constraints are imposed on deception signals to ensure the physical feasibility of the attack scenario.
4. A Markov jump process is incorporated into the controller to model the stochastic evolution of controller faults. This approach enables dynamic switching between different fault modes and improves system fault tolerance under controller degradation.

Figure 1 depicts the overall architecture of the proposed observer-based noncollocated fuzzy boundary control system. Table 1 provides a feature-level comparison between representative related works and this study in terms of BW, Atk, FT and Dist, highlighting that the proposed method integrates these practical design features in a unified framework.

Notes: T–S—Takagi–Sugeno fuzzy modelling/control framework; BW—bandwidth saving via improved sampling/event-triggering; Atk—cyber-attacks (e.g., DoS/deception/replay and so on); FT—fault-tolerant control (sensor/actuator/controller faults) and Dist—external disturbance/noise or explicit performance index (e.g., H_∞).

Notation: $\mathcal{H}^n \triangleq \mathcal{L}_2([l_1, l_2]; \mathbb{R}^n)$ denotes the Hilbert space consisting of square-integrable vector functions $\vartheta(r, \cdot)$ over the interval $[l_1, l_2]$. Let $r \in [l_1, l_2] \subset \mathbb{R}$ and $t \geq 0$. The inner product and norm are defined as follows:

$$\langle \vartheta_1(r, \cdot), \vartheta_2(r, \cdot) \rangle = \int_{l_1}^{l_2} \|\vartheta_1(r, \cdot)\|_2^2 \, dr,$$

and

$$\|\vartheta_1(r, \cdot)\|_2 = \sqrt{\int_{l_1}^{l_2} \|\vartheta_1(r, \cdot)\|_2^2 \, dr},$$

where $\vartheta_1(r, \cdot), \vartheta_2(r, \cdot) \in \mathcal{H}^n$. $\mathcal{W}^{l,2}([l_1, l_2]; \mathbb{R}^n)$ denotes the n-dimensional Sobolev space consisting of vector functions $\varpi(r) : [l_1, l_2] \to \mathbb{R}^n$ with square-integrable weak derivatives up to order $l \geq 1$. The norm in this space is defined as follows:

$$\|\varpi(r, \cdot)\|_{\mathcal{W}^{l,2}}^2 = \int_{l_1}^{l_2} \sum_{i=0}^{l} \left(\frac{\partial^i \varpi(r, \cdot)}{\partial r^i} \right)^{\mathrm{T}} \left(\frac{\partial^i \varpi(r, \cdot)}{\partial r^i} \right) dr.$$

The partial derivative is defined as $\vartheta_t(r, t) \triangleq \frac{\partial \vartheta(r,t)}{\partial t}$, $\vartheta_r(r, t) \triangleq \frac{\partial \vartheta(r,t)}{\partial r}$ and $\vartheta_{rr}(r, t) \triangleq \frac{\partial \vartheta^2(r,t)}{\partial r^2}$.

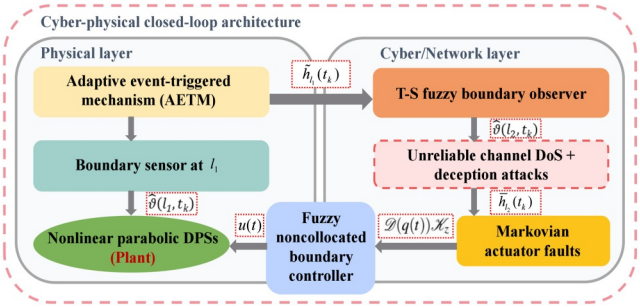


FIGURE 1 | Overall structure of the proposed observer-based noncollocated fuzzy boundary control system under hybrid attacks and Markovian actuator failures.

2 | Preliminaries

2.1 | T–S Fuzzy Modelling of the DPSs

This paper considers the DPSs with time-varying delays expressed as follows:

$$\begin{cases} \vartheta_t(r, t) = \{\Upsilon \vartheta_r(r, t)\}_r + f(\vartheta(r, t), \vartheta(r, t - \tau(t))) \\ \qquad\qquad + g(\vartheta(r, t))\omega(r, t), \\ \vartheta(r, 0) = \vartheta_0(r), \\ \vartheta_r(r, t)|_{r=l_1} = 0, \\ \vartheta_r(r, t)|_{r=l_2} = Bu(t). \end{cases} \tag{1}$$

The state $\vartheta(r, t) \in \mathbb{R}^{n_\vartheta}$ evolves over the domain $r \in [l_1, l_2] \subset \mathbb{R}$ and time $t \geq -\lambda$, where r and t represent space and time, respectively. Within this domain, a bounded disturbance $\omega(r, t) \in \mathbb{R}^{n_\omega}$ is present. The nonlinear functions $f(\cdot)$ and $g(\cdot)$ satisfy the Lipschitz condition, and the matrix Υ satisfies $0 < \Upsilon \in \mathbb{R}^{n_\vartheta \times n_\vartheta}$. The system is driven by the input $u(t) \in \mathbb{R}^{n_u}$, with initial condition $\vartheta_0(r) \in \mathbb{R}^{n_\vartheta}$. The delay $\tau(t)$ is differentiable and bounded by $0 \leq \tau(t) \leq \overline{\tau}$, with $\dot{\tau}(t) \leq \overline{\tau} < 1$.

Plant Rule i: IF $\delta_1(r, t)$ is θ_1^i, ..., and $\delta_n(r, t)$ is θ_n^i, THEN

$$\begin{aligned} \vartheta_t(r, t) =& \{\Upsilon \vartheta_r(r, t)\}_r + (\mathcal{A}_i \vartheta(r, t) + \mathcal{A}_{di} \vartheta(r, t - \tau(t)) \\ &+ \mathcal{F}_i \omega(r, t)), \end{aligned} \tag{2}$$

where $\delta_1(r, t), ..., \delta_n(r, t)$ denotes the premise variables and θ_l^i and $l = 1, ..., n$ represent the associated fuzzy sets. The matrices $\mathcal{A}_i$, $\mathcal{A}_{di}$ and $\mathcal{F}_i$ are known for each rule i in the index set $\mathbb{M} = \{1, 2, ..., m\}$. Accordingly, Equation (2) can be reformulated as follows:

$$\begin{aligned} \vartheta_t(r, t) = \{\Upsilon \vartheta_r(r, t)\}_r + \sum_{i=1}^{m} \mathcal{W}_i(\delta(r, t))(\mathcal{A}_i \vartheta(r, t) \\ + \mathcal{A}_{di} \vartheta(r, t - \tau(t)) + \mathcal{F}_i \omega(r, t)), \end{aligned} \tag{3}$$

TABLE 1 | Feature-level comparison of representative related works and this study.

Ref	Method/focus	T–S	BW	Atk	FT	Dist
[17]	Fuzzy noncollocated boundary control under random sensor faults	✓	—	—	—	✓
[18]	Fuzzy boundary sampled-data control with random time-varying delays	✓	—	—	—	—
[19]	Observer-based H_∞ sampled-data fuzzy control	✓	—	—	—	✓
[20]	Fault tolerant stochastic sampled-data fuzzy control	✓	—	—	✓	—
[21]	Sampled-data-based event-triggered fuzzy control under cyberattacks	—	✓	✓	—	—
[22]	Observer-based periodic event-triggered and self-triggered boundary control	—	✓	—	—	—
[27]	Fault-tolerant ETSD fuzzy control under pointwise/limited measurements	✓	✓	—	✓	—
[31]	Fuzzy fault-tolerant boundary control under stochastic actuator failures	✓	—	—	✓	—
[32]	Adaptive actuator failure compensation control	—	—	—	✓	—
[34]	ETSD fuzzy secure control under deception attacks and random failures	✓	✓	✓	✓	—
This study	Secure fault-tolerant AETM-based T–S fuzzy boundary output-feedback control	✓	✓	✓	✓	✓

where

$$\delta(r,t) = [\delta_1(r,t), ..., \delta_n(r,t)]^{\mathrm{T}},$$

$$\mathcal{W}_i(\delta(r,t)) = \frac{\mathcal{H}_i(\delta(r,t))}{\sum_{i=1}^{m} \mathcal{H}_i(\delta(r,t))},$$

$$\mathcal{H}_i(\delta(r,t)) = \prod_{l=1}^{n} \theta_l^i(\delta_l(r,t)),$$

with the normalised membership functions $\mathcal{W}_i(\delta(r,t))$ satisfying

$$\mathcal{W}_i(\delta(r,t)) \geqslant 0, \ \sum_{i=1}^{m} \mathcal{W}_i(\delta(r,t)) = 1, \ i \in \mathbb{M}. \tag{4}$$

In summary, the fuzzy rule in Equation (2) together with the normalised membership functions in Equation (4) yields the global T–S fuzzy parabolic model in Equation (3). The local matrices $\mathcal{A}_i$, $\mathcal{A}_{di}$ and $\mathcal{F}_i$ characterise the dynamics under each rule and are directly used as the plant matrices in the subsequent boundary observer and noncollocated fuzzy NBSDC synthesis.

Remark 1. The above model Equation (1) describes a class of parabolic DPSs with time-varying delays. These systems are inherently infinite-dimensional and are typically modelled by second-order PDEs to capture spatiotemporal behaviours. The formulation accounts for nonlinear dynamics, delayed feedback, spatial diffusion and boundary actuation, which are commonly encountered in practical systems. Notably, such a model is capable of representing tumour cell diffusion processes [36] as well as the FitzHugh–Nagumo (FHN) equation, which characterises wave propagation phenomena in biological [37] and chemical environments [38].

In terms of methodology, compared with general nonfuzzy PDE boundary control designs, the adopted T–S fuzzy representation provides a systematic way to handle nonlinearities and delay effects, leading to an LMI-based synthesis with a prescribed H_∞ performance level under limited and noncollocated boundary measurements. In contrast to standard fuzzy schemes that often assume periodic sampling and attack-/fault-free channels, the present framework incorporates adaptive event-triggered bandwidth saving and explicit robustness against hybrid cyber-attacks and Markovian actuator faults, thereby improving practical deployability under realistic network conditions.

2.2 | Adaptive Event-Triggered Control Scheme

The sensor can provide the following BMs:

$$h_r(t_k) = \vartheta(r, t_k), \tag{5}$$

where r is defined over the closed interval $[l_1, l_2] \subset \mathbb{R}$ and $0 = t_0 < t_1 < \cdots < t_k < \cdots < \lim_{k\to\infty} t_k = \infty$ are the sampling time instants.

Distinct from conventional event-triggered control principles, the proposed AETM in Equation (5) employs a time-varying threshold to suppress redundant data transmissions in nonlinear parabolic DPSs. At each sampling instant, the mechanism compares the newly sampled boundary measurement with the last transmitted one and triggers an update only when the difference exceeds the current threshold; the next triggering time instant t_{k+1} is determined by

$$t_{k+1} = \min_{h\geq 1}\{t_k^i | e_k^T(t)\Phi e_k(t) \geq \sigma(t) h_r^T(t_k)\Phi h_r(t_k)\}, \tag{6}$$

in which t_k (for $k = 0, 1, 2, ...$) denotes the sequence of release instants, with the initial value $t_0 = 0$. The variable t_k^i refers to the current sampling instant. The error signal is defined as $e_k(t) = h_r(t_k) - h_r(t_k^i)$, where $h_r(t_k)$ denotes the latest triggered signal and $h_r(t_k^i)$ denotes the current sampled signal. Φ is a positive definite weighting matrix determined through design, and the triggering threshold function $\sigma(t) \in [0, 1]$ is time-varying defined as follows:

$$\sigma(t) = \underline{\sigma} + (\overline{\sigma} - \underline{\sigma})\exp\left(-\lambda e_k^T(t) e_k(t)\right), \tag{7}$$

where $\overline{\sigma}$ and $\underline{\sigma}$ represent the upper and lower limits of $\sigma(t)$, respectively. $\lambda > 0$ denotes the impact coefficient of the state error.

$$\tilde{h}_r(t_k) = \begin{cases} h_r(t_k^i), & \text{if condition (7) holds,} \\ h_r(t_k), & \text{if condition (7) does not hold,} \end{cases} \tag{8}$$

in which $\tilde{h}_r(t_k)$ denotes the actual control signal to be transmitted or executed at the triggering instant t_k.

Remark 2. Compared with ETMs in refs. [27, 34], which use constant thresholds based on a fixed β_s, the proposed AETM in Equations (6–8) employs a time-varying threshold $\sigma(t)$ that adapts to the estimation error. Letting $\sigma(t)$ decay exponentially with the error norm makes the triggering rule more adaptive. This strategy suppresses redundant transmissions and yields a more balanced use of communication resources. In practice, the triggering condition is relaxed during quasi-steady operation and tightened under transients or attack-induced anomalies, which mitigates the trade-off in fixed-threshold schemes between conservative tuning and performance.

2.3 | Research Problem Statement and Formulation

Based on the T–S fuzzy representation in Equation (3) and the adaptive event-triggered scheme in Equations (6–8), we now formulate the overall observer–controller structure for the nonlinear parabolic DPSs. Departing from the central sensor placement adopted [27], where sensors are positioned at the centre of each subdomain Ω_s, this study considers boundary-mounted sensors, which directly capture the following noncollocated estimated BMs

$$\hat{h}_{l_1}(t_k) = \hat{\vartheta}(l_1, t_k). \tag{9}$$

Utilising the BMs defined in Equation (9), the corresponding fuzzy observer model is constructed as follows:

Observer rule j: IF $\hat{\delta}_1(r, t_k)$ is θ_1^j, ..., and $\hat{\delta}_n(r, t_k)$ is θ_n^j, **THEN**

$$\begin{cases} \dot{\hat{\vartheta}}_t(r,t) = \left\{\Upsilon\hat{\vartheta}_r(r,t)\right\}_r + \mathcal{A}_j\hat{\vartheta}(r,t) \\ \qquad\qquad + \mathcal{A}_{dj}\hat{\vartheta}(r,t-\tau(t)) \\ \qquad\qquad + \mathcal{I}_j\left(\tilde{h}_{l_1}(t_k) - \hat{h}_{l_1}(t_k)\right), \\ \hat{\vartheta}(r,0) = \hat{\vartheta}_0(r), \\ \hat{\vartheta}_r(r,t)|_{r=l_1} = \mathcal{L}_j\left(\tilde{h}_{l_1}(t_k) - \hat{h}_{l_1}(t_k)\right), \\ \hat{\vartheta}_r(r,t)|_{r=l_2} = \mathcal{B}u(t), \end{cases} \tag{10}$$

where $\hat{\vartheta}(r,t) \in \mathbb{R}^{n_\vartheta}$ denotes the estimated state and $\hat{\vartheta}_0(r) \in \mathbb{R}^{n_\vartheta}$ is its initial value. The signal $\tilde{h}_r(t_k) \in \mathbb{R}^{n_h}$ represents the final measured output fed to the observer, whereas $\hat{h}_r(t_k) \in \mathbb{R}^{n_\vartheta}$ denotes the estimated BMs signal. The matrices $\mathcal{I}_j \in \mathbb{R}^{n_\vartheta \times n_\vartheta}$ and $\mathcal{L}_j \in \mathbb{R}^{n_\vartheta \times n_\vartheta}$ denote the observer gains, and $\hat{\delta}_1(r,t_k), ..., \hat{\delta}_n(r,t_k)$ are the premise variables of the fuzzy observer.

Denote $e(r,t_k) \triangleq \vartheta(r,t_k) - \hat{\vartheta}(r,t_k)$ and $h_{e,r}(t_k) = \mathcal{L}_j\left(\tilde{h}_r(t_k) - \hat{h}_r(t_k)\right)$. To further describe the observer output of the estimated parabolic DPSs in Equation (10), the following definition is introduced:

$$h_{e,l_1}(t_k) = \sum_{j=1}^{m} \mathcal{W}_j\left(\hat{\delta}(r,t_k)\right)\mathcal{L}_j e(l_1,t_k). \tag{11}$$

Assume that hybrid attacks occur at the boundary l_2 with a certain probability. The received output is represented as follows:

$$\overline{h}_{l_2}(t_k) = (1-\alpha)(1-\beta)\hat{h}_{l_2}(t_k) + \alpha(1-\beta)f\left(\hat{h}_{l_2}(t_k)\right), \tag{12}$$

where α and β denote the occurrence probabilities of deception and DoS attacks, respectively. Both variables follow Bernoulli distributions with expectations $\mathbb{E}\{\alpha\} = \overline{\alpha}$ and $\mathbb{E}\{\beta\} = \overline{\beta}$. Moreover, deception attack signals are limited by energy as follows:

$$\|f\left(\hat{h}_{l_2}(t_k)\right)\|_2 \le \|C\hat{h}_{l_2}(t_k)\|_2. \tag{13}$$

Remark 3. Unlike the conventional boundary observer framework in ref. [19], which assumes secure communication channels, this study introduces a hybrid attack model at boundary point l_2 to better reflect realistic networked environments. The received output may be the nominal signal, a falsified signal generated by a deception attack or a missing signal caused by a DoS attack. These switching patterns produce mismatched measurements that can arise in networked industrial processes and biomedical diffusion systems. The deceptive signal $f\left(\hat{h}_{l_2}(t_k)\right)$ deviates from the true output, whereas the DoS case completely removes information and its energy is constrained by the bound in Equation (13). In addition, the state information at boundary point l_1 is incomplete, so a fuzzy BMs model based on the estimation error is constructed in Equation (11) to dynamically compensate boundary disturbances. Overall, the proposed design enhances robustness against cyber-attacks with mismatched signals. However, the hybrid model relies on known bounds on the attack energy and assumes a single active attack type at each sampling instant, and it does not capture more sophisticated coordinated or stealthy attacks, which limits its applicability in networked DPSs studies.

In practical industrial environments, maintaining system stability under actuator failure conditions is essential. To characterise actuator failure behaviour, the system described in Equation (2) with BMs Equation (12) can be modelled using the following failure representation:

Controller rule z: IF $\hat{\delta}_1(l_2,t_k)$ is θ_1^z, ..., and $\hat{\delta}_n(l_2,t_k)$ is θ_n^z, THEN

$$u(t) = \mathcal{D}(q(t))\mathcal{K}_z\overline{h}_{l_2}(t_k), \tag{14}$$

where $\mathcal{K}_z \in \mathbb{R}^{n_u \times n_r}$ represents the intended control gains. $\mathcal{D}(q(t)) = \mathrm{diag}\{d_1(q(t)), d_2(q(t)), ..., d_k(q(t))\}$, $d_g(q(t)) \in [0,1]$ and $g \triangleq 1, 2, ..., k$. Define $q(t)$ as a right-continuous Markov chain, independent of other processes, with state space $\mathcal{S} = \{1, 2, ..., s\}$. This Markov jump process models random switching among a finite number of actuator conditions (such as normal, partially degraded or failed), where the transition rates π_{cd} describe how likely the system is to move from one condition to another over time. Its infinitesimal generator is denoted by $\Pi = [\pi_{cd}]_{s\times s}$, and the transition probabilities are specified as follows:

$$\Pr\left\{q_{t+\chi} = d | q_t = c\right\} = \begin{cases} \pi_{cd}\chi + o(\chi), & c \ne d, \\ 1 + \pi_{cc}\chi + o(\chi), & c = d, \end{cases} \tag{15}$$

in which $\chi > 0$, $\lim_{\chi\to 0}(o(\chi)/\chi) = 0$, $\pi_{cd} > 0$, $c \ne d$ and $\pi_{cc} = -\sum_{c=1, d\ne c}^{s}\pi_{cd}$, for $\forall\, c \in \mathcal{S}$.

It is straightforward to classify the sensor status into the following cases:

1. $d_g(q(t)) = 1$, sensor operates normally without faults.
2. $0 < d_g(q(t)) < 1$, partial degradation of sensor functionality.
3. $d_g(q(t)) = 0$, complete sensor failure.

For simplicity, denote $\mathcal{D}_q = \mathcal{D}(q(t))$ and the observer-based fuzzy noncollocated ETSD controller is described as follows:

$$\begin{aligned} u(t) = \sum_{z=1}^{m} \mathcal{W}_z\left(\hat{\delta}(l_2,t_k)\right)\mathcal{D}_q\mathcal{K}_z\Big[&(1-\alpha)(1-\beta)\hat{\vartheta}(l_2,t_k) \\ &+ \alpha(1-\beta)f\left(\hat{h}_{l_2}(t_k)\right)\Big]. \end{aligned} \tag{16}$$

Remark 4. The controller is developed under a noncollocated boundary control framework, where sensing and actuation are located at different boundary points. In practice, the boundary point l_1 is relatively secure and locally accessible, but the sensor at l_1 can only provide partial information due to limited BMs. By contrast, the boundary point l_2 is less secure and typically lacks direct measurements, so the controller at l_2 cannot use the actual boundary values. To address this, the observer in Equation (10) is introduced to estimate the state online. The sensor at l_1 generates the error signal $e(l_1,t_k)$, and the observer-based estimate $\hat{h}_{l_2}(t_k)$ is

used as the reference for control. Since $\hat{h}_{l_2}(t_k)$ is transmitted through a vulnerable channel, it may be corrupted by deception or DoS attacks. Therefore, the signal received at l_2 is $\overline{h}_{l_2}(t_k)$ in Equation (12), which accounts for both the observer output and cyber-attacks. Based on $\overline{h}_{l_2}(t_k)$, the control input in Equation (14) is constructed, ensuring implementability under limited BMs and insecure communication conditions.

Remark 5. In Equation (6) of ref. [35], sensor and controller malfunctions are only described in a simplified way through intermittent measurements. By contrast, the proposed non-collocated structure in Equation (14) integrates a robust observer with controller coordination, providing a more practical framework. This work explicitly considers the effects of cyber-attacks and random failures, which can lead to unmeasurable or partially measurable boundary states. As a result, the formulation provides a closer representation of the sensing and communication constraints in networked DPSs.

Substituting Equation (16) into Equation (3), we have

$$\begin{cases} \vartheta_t(r,t) = \{\Upsilon\vartheta_r(r,t)\}_r + \sum_{i=1}^{m} \mathcal{W}_i(\delta(r,t))(\mathcal{A}_i\vartheta(r,t) \\ \qquad + \mathcal{A}_{di}\vartheta(r,t-\tau(t)) + \mathcal{F}_i\omega(r,t)), \\ \vartheta(r,0) = \vartheta_0(r), \\ \vartheta_r(r,t)|_{r=l_1} = 0, \\ \vartheta_r(r,t)|_{r=l_2} = \sum_{z=1}^{m} \mathcal{W}_z\Big(\hat{\delta}(l_2,t_k)\Big)\mathcal{D}_q\mathcal{B}\mathcal{K}_z \\ \qquad \Big[(1-\alpha)(1-\beta)\hat{\vartheta}(l_2,t_k) \\ \qquad + \alpha(1-\beta)f\Big(\hat{h}_{l_2}(t_k)\Big)\Big]. \end{cases} \tag{17}$$

Based on the fuzzy BMs defined in Equation (11), the final observer for the DPSs in Equation (1) is formulated as follows:

$$\begin{cases} \hat{\vartheta}_t(r,t) = \Big\{\Upsilon\hat{\vartheta}_r(r,t)\Big\}_r + \sum_{j=1}^{m} \mathcal{W}_j\Big(\hat{\delta}(r,t_k)\Big) \\ \qquad \Big(\mathcal{A}_j\hat{\vartheta}(r,t) + \mathcal{A}_{dj}\hat{\vartheta}(r,t-\tau(t)) \\ \qquad + \mathcal{I}_j e(l_1,t_k)\Big), \\ \hat{\vartheta}(r,0) = \hat{\vartheta}_0(r), \\ \hat{\vartheta}_r(r,t)|_{r=l_1} = -\sum_{j=1}^{m} \mathcal{W}_j\Big(\hat{\delta}(r,t_k)\Big)\mathcal{L}_j e(l_1,t_k), \\ \hat{\vartheta}_r(r,t)|_{r=l_2} = \sum_{z=1}^{m} \mathcal{W}_z\Big(\hat{\delta}(l_2,t_k)\Big)\mathcal{D}_q\mathcal{B}\mathcal{K}_z \\ \qquad \Big[(1-\alpha)(1-\beta)\hat{\vartheta}(l_2,t_k) \\ \qquad + \alpha(1-\beta)f\Big(\hat{h}_{l_2}(t_k)\Big)\Big]. \end{cases} \tag{18}$$

The estimation error associated with the fuzzy DPSs is derived based on Equations (17) and (18) as follows:

$$\begin{cases} e_t(r,t) = \{\Upsilon e_r(r,t)\}_r \\ \qquad + \sum_{i=1}^{m}\sum_{j=1}^{m} \mathcal{W}_i(\delta(r,t_k))\mathcal{W}_j\Big(\hat{\delta}(r,t_k)\Big) \\ \qquad \big(\mathcal{A}_j e(r,t) + \mathcal{A}_{dj}e(r,t-\tau(t)) \\ \qquad - \mathcal{I}_j e(l_1,t_k) + \mathcal{F}_i\overline{\omega}(r,t)\big), \\ e(r,0) = e_0(r), \\ e_r(r,t)|_{r=l_1} = -\sum_{j=1}^{m} \mathcal{W}_j\Big(\hat{\delta}(r,t_k)\Big)\mathcal{L}_j e(l_1,t_k), \\ e_r(r,t)|_{r=l_2} = 0. \end{cases} \tag{19}$$

in which $e_0(r) \triangleq \delta_0(r) - \hat{\delta}_0(r)$, $\mathcal{F}_i = [\mathcal{F}_i\ I]$, $\overline{\omega}(r,t) = \big[\omega^{\mathrm{T}}(r,t), \omega_0^{\mathrm{T}}(r,t)\big]^{\mathrm{T}}$ and $\omega_0(r,t) = \Big\{\sum_{i=1}^{m}\mathcal{W}_i(\delta(r,t))\mathcal{A}_i - \sum_{j=1}^{m}\mathcal{W}_j\Big(\hat{\delta}(r,t_k)\Big)\mathcal{A}_j\Big\}\vartheta(r,t)$ is regarded as a disturbance term introduced by the approximation error of fuzzy modelling.

In order to reduce the disturbance caused by $\overline{\omega}(r,t)$, an H_∞ performance index is considered for system Equation (19):

$$\begin{aligned} &\int_{t_0}^{+\infty}\int_{\Psi} \overline{\vartheta}^{\mathrm{T}}(r,t)\overline{\mathcal{O}}\,\overline{\vartheta}(r,t)drdt \\ &\leqslant \gamma^2\int_{t_0}^{+\infty}\int_{\Psi} \overline{\omega}^{\mathrm{T}}(r,t)\overline{\omega}(r,t)drdt, \end{aligned} \tag{20}$$

where $\overline{\vartheta}(r,t) = \big[\vartheta^{\mathrm{T}}(r,t),\ e^{\mathrm{T}}(r,t)\big]^{\mathrm{T}}$, $\overline{\mathcal{O}} = \big[\mathcal{O}_1^{\mathrm{T}},\ \mathcal{O}_2^{\mathrm{T}}\big]^{\mathrm{T}}$, the attenuation parameter is specified as $\gamma > 0$, with $\mathcal{O} \in \mathbb{R}^{n_\vartheta \times n_\vartheta}$.

Remark 6. Compared with refs. [19, 20], which mainly treat bounded external inputs in sampled-data fuzzy observer design for nonlinear parabolic PDEs, a more implementation-oriented disturbance description is adopted here. The term $\overline{\omega}(r,t)$ in Equation (19) is decomposed into the physical perturbation $\omega(r,t)$ and a mismatch term $\omega_0(r,t)$ that represents plant–fuzzy approximation errors. This decomposition allows the LKFs to account for both environmental uncertainties and modelling imperfections. In practice, once bounds on $\omega(r,t)$ and $\omega_0(r,t)$ are available, the weighting matrices can be tuned to balance disturbance attenuation and robustness against model-plant mismatches.

Based on this disturbance description, the LKFs are constructed from a practical viewpoint to capture key features of networked parabolic DPSs, including spatially distributed dynamics, time-varying delays and sampled-data observations. With $\overline{\omega}(r,t)$ embedded, the LKFs consist of boundary-energy terms, delay-dependent integral terms and sampling-related terms, which lead to LMI conditions that remain computationally tractable. The results are established under explicit assumptions, including bounded delays, known bounds on

disturbances and modelling errors and noncollocated, but fixed boundary measurements. Under these assumptions, the closed-loop estimation error system satisfies the mean-square H_∞ requirement in Equation (20). Accordingly, the applicability is clear, and the validity is confined to systems that meet the above modelling conditions.

Assumption 1. [31] For the given matrices, $\zeta_1 > 0$, $\zeta_2 > 0$ and $\zeta_3 > 0$, the following inequality holds:

$$\begin{aligned}\mathcal{G}(t) \triangleq & \int_\Psi \vartheta^{\mathrm{T}}(r,t)\zeta_1\vartheta(r,t)dr + \int_\Psi \vartheta_t^{\mathrm{T}}(r,t)\zeta_2\vartheta_t(r,t)dr \\ & + \vartheta^{\mathrm{T}}(l_2,t)\zeta_3\vartheta(l_2,t) - \vartheta_t^{\mathrm{T}}(l_2,t)\vartheta_t(l_2,t) \geqslant 0.\end{aligned} \tag{21}$$

Lemma 1. *[17] For a vector function $\vartheta \in \mathcal{H}^{n_\vartheta}$ with $\vartheta(l_1) = 0$ or $\vartheta(l_2) = 0$, one can establish the inequality below for any matrix $\mathcal{M} \geqslant 0$:*

$$\begin{aligned}&\int_\Psi \vartheta^{\mathrm{T}}(t)\mathcal{M}\vartheta(t)dt \\ &\leqslant \frac{4(l_2-l_1)^2}{\pi^2}\int_\Psi \left[\frac{d\vartheta}{dt}\right]^{\mathrm{T}}\mathcal{M}\left[\frac{d\vartheta}{dt}\right]dt.\end{aligned} \tag{22}$$

Moreover, if $\vartheta(l_1) = 0$ and

$$\begin{aligned}&\int_\Psi \vartheta^{\mathrm{T}}(t)\mathcal{M}\vartheta(t)dt \\ &\leqslant \frac{(l_2-l_1)^2}{\pi^2}\int_\Psi \left[\frac{d\vartheta}{dt}\right]^{\mathrm{T}}\mathcal{M}\left[\frac{d\vartheta}{dt}\right]dt.\end{aligned} \tag{23}$$

Lemma 2. *[27] Given a matrix $\mathcal{M} \geqslant 0$, a scalar $\overline{\tau} > 0$ and a vector function $\vartheta \in \mathcal{H}^{n_\vartheta}$, the following inequality holds:*

$$\begin{aligned}&\overline{\tau}\int_\Psi\int_{t-\overline{\tau}}^{t}\vartheta^{\mathrm{T}}(r,t)\mathcal{M}\vartheta(r,t)drdt \\ &\geqslant \int_\Psi\left(\int_{t-\overline{\tau}}^{t}\vartheta^{\mathrm{T}}(r,t)dt\right)\mathcal{M}\left(\int_{t-\overline{\tau}}^{t}\vartheta(r,t)dt\right)dr.\end{aligned} \tag{24}$$

3 | Main Results

This section focuses on the H_∞ FNSDO design for the fuzzy DPSs Equation (17) and its estimation error system Equation (19) based on LKFs. The analysis begins with the following LKFs:

$$V(t) = \sum_{i=1}^{7}\mathcal{V}_i(t), \tag{25}$$

where

$$\mathcal{V}_1(t) = \int_\Psi \varepsilon_1^{\mathrm{T}}(r,t)\mathcal{P}_1\varepsilon_1(r,t)dr,$$

$$\mathcal{V}_2(t) = \int_\Psi \varepsilon_2^{\mathrm{T}}(r,t)\mathcal{P}_2\varepsilon_2(r,t)dr,$$

$$\mathcal{V}_3(t) = \rho(t)\int_\Psi \left[\varepsilon_3^{\mathrm{T}}(r,t)\mathcal{S}_1\varepsilon_3(r,t) + 2\varepsilon_4^{\mathrm{T}}(r,t)\mathcal{S}_2\varepsilon_3(r,t)\right]dr,$$

$$\mathcal{V}_4(t) = \rho(t)\int_\Psi\int_{t_k}^{t} e^{2\delta(v-t)}\varepsilon_5^{\mathrm{T}}(r,s)\mathcal{R}\varepsilon_5(r,s)dsdr,$$

$$\mathcal{V}_5(t) = \int_\Psi\int_{t-\overline{\tau}}^{t} e^{2\delta(v-t)}\varepsilon_6(r,s)^{\mathrm{T}}\mathcal{X}_1\varepsilon_6(r,s)dsdr,$$

$$\mathcal{V}_6(t) = \int_\Psi\int_{t-\tau(t)}^{t} e^{2\delta(v-t)}\varepsilon_6(r,s)^{\mathrm{T}}\mathcal{X}_2\varepsilon_6(r,s)dsdr,$$

$$\mathcal{V}_7(t) = \overline{\tau}\int_\Psi\int_{t-\overline{\tau}}^{t}\int_{\varphi}^{t} \mathrm{e}^{2\delta(v-t)}\varepsilon_7(r,s)^{\mathrm{T}}\mathcal{X}_3\varepsilon_7(r,s)dsd\varphi dr,$$

in which $\varepsilon_1(r,t) = \mathrm{col}\{\vartheta(r,t), e(r,t)\}$, $\varepsilon_2(r,t) = \mathrm{col}\{\vartheta_r(r,t), e_r(r,t)\}$, $\varepsilon_3(r,t) = \mathrm{col}\left\{\tilde{\vartheta}(r,t), \tilde{e}(r,t)\right\}$, $\varepsilon_4(r,t) = \mathrm{col}\left\{\vartheta(r,t) - \tilde{\vartheta}(r,t),\ e(r,t) - \tilde{e}(r,t)\right\}$, $\varepsilon_5(r,s) = \mathrm{col}\{\zeta(r,s), \eta(r,s)\}$, $\varepsilon_6(r,s) = \mathrm{col}\{\vartheta(r,s), e(r,s)\}$, $\varepsilon_7(r,s) = \mathrm{col}\{\vartheta_s(r,s), e_s(r,s)\}$, $\rho(t) = t_{k+1} - t$, $\tilde{\vartheta}(r,t) = \vartheta(r,t) - \vartheta(r,t_k)$, $\tilde{e}(r,t) = e(r,t) - e(r,t_k)$, $\mathcal{P}_1 = \begin{bmatrix}\mathcal{Z}_1 & 0\\ 0 & \mathcal{U}_a\end{bmatrix}$, $\mathcal{P}_2 = \begin{bmatrix}\mathcal{Z}_2^{\mathrm{T}}\Upsilon & 0\\ 0 & \mathcal{U}_2^{\mathrm{T}}\Upsilon\end{bmatrix}$, $\mathcal{R} = \begin{bmatrix}\mathcal{M} & 0\\ 0 & \mathcal{N}\end{bmatrix}$, $\mathcal{M} = \begin{bmatrix}\mathcal{M}_{11} & \mathcal{M}_{12}\\ * & \mathcal{M}_{22}\end{bmatrix}$, $\mathcal{N} = \begin{bmatrix}\mathcal{N}_{11} & \mathcal{N}_{12}\\ * & \mathcal{N}_{22}\end{bmatrix}$, $\mathcal{S}_f = \begin{bmatrix}\mathcal{R}_f & 0\\ 0 & \mathcal{Q}_f\end{bmatrix}$, $\mathcal{X}_k = \begin{bmatrix}\mathcal{J}_k & 0\\ 0 & \mathcal{H}_k\end{bmatrix}$, and $\delta > 0$, $\overline{\tau} > 0$, $0 < \mathcal{P}_1 \in \mathbb{R}^{2n_\vartheta \times 2n_\vartheta}$, $\mathcal{P}_2 \in \mathbb{R}^{2n_\vartheta \times 2n_\vartheta}$ satisfies $0 < \mathcal{P}_2 = \mathcal{P}_2^{\mathrm{T}}$, $0 < \mathcal{M}, \mathcal{N} \in \mathbb{R}^{2n_\vartheta \times 2n_\vartheta}$, $0 < \mathcal{R} \in \mathbb{R}^{4n_\vartheta \times 4n_\vartheta}$, $0 < \mathcal{S}_1$, $\mathcal{S}_2 \in \mathbb{R}^{2n_\vartheta \times 2n_\vartheta}$ satisfies $\mathcal{S}_1 = \mathcal{S}_1^{\mathrm{T}}$, $0 < \mathcal{X}_k \in \mathbb{R}^{2n_\vartheta \times 2n_\vartheta}$, $f = 1, 2$, $k = 1, 2, 3$.

Remark 7. The augmented terms $\mathcal{V}_4(t)$–$\mathcal{V}_7(t)$ in the LKFs of Equation (25) are delay-dependent and include an exponential weighting $\mathrm{e}^{2\delta(v-t)}$ ($\delta > 0$). This design reduces conservatism in stability analysis when time-varying delays are present. These terms are introduced to capture historical state information across spatial and temporal domains, which improves robustness under irregular sampling and BMs. In contrast to traditional ODE-based methods [13–15, 36–38], the proposed framework effectively addresses spatially distributed nonlinear terms such as $\{\Upsilon\vartheta_r(r,t)\}_r$ and $\{\Upsilon e_r(r,t)\}_r$ as well as Markov jump characteristics. This provides a solid basis for H_∞ FNSDO design.

Proposition 1. *Assume that there exist $\mathcal{Z}_1 > 0$, $\mathcal{R}_1 = \mathcal{R}_1^{\mathrm{T}}$, $\mathcal{R}_2$, $\mathcal{M} > 0$, $\mathcal{U}_a > 0$, $\mathcal{Q}_1 = \mathcal{Q}_1^{\mathrm{T}}$, $\mathcal{Q}_2$, $\mathcal{N} > 0$, $\mathcal{W}_1 \in \mathbb{R}^{n_\vartheta \times n_\vartheta}$, $\mathcal{W}_2 \in \mathbb{R}^{n_\vartheta \times n_\vartheta}$, $\mathcal{E}_1 \in \mathbb{R}^{n_\vartheta \times n_\vartheta}$ and $\mathcal{E}_2 \in \mathbb{R}^{n_\vartheta \times n_\vartheta}$, such that the following LMIs hold:*

$$\Theta_\iota(m) > 0, \iota = 1, 2, 3, 4, \tag{26}$$

where

$$\Theta_1(m)=\begin{bmatrix}\Theta_1^{11}(m) & \Theta_1^{12}(m)\\ * & \Theta_1^{22}(m)\end{bmatrix},$$

$$\Theta_2(m)=\begin{bmatrix}\Theta_2^{11}(m) & \Theta_2^{12}(m) & \Theta_2^{13}(m)\\ * & \Theta_2^{22}(m) & \Theta_2^{23}(m)\\ * & * & \Theta_2^{33}(m)\end{bmatrix},$$

$$\Theta_3(m)=\begin{bmatrix}\Theta_3^{11}(m) & \Theta_3^{12}(m)\\ * & \Theta_3^{22}(m)\end{bmatrix},$$

$$\Theta_4(m)=\begin{bmatrix}\Theta_4^{11}(m) & \Theta_4^{12}(m) & \Theta_4^{13}(m)\\ * & \Theta_4^{22}(m) & \Theta_4^{23}(m)\\ * & * & \Theta_4^{33}(m)\end{bmatrix},$$

$$\Theta_1^{11}(m)=\mathcal{Z}_1+m\mathcal{R}_1+m\{\mathcal{W}_1+\mathcal{W}_1^{\mathrm{T}}\},$$
$$\Theta_1^{12}(m)=-m\mathcal{R}_1+m\mathcal{R}_2^{\mathrm{T}}+m\{-\mathcal{W}_1+\mathcal{W}_2^{\mathrm{T}}\},$$
$$\Theta_1^{22}(m)=m\mathcal{R}_1-m\{\mathcal{R}_1+\mathcal{R}_2^{\mathrm{T}}\}-m\{\mathcal{W}_1+\mathcal{W}_2^{\mathrm{T}}\},$$
$$\Theta_2^{11}(m)=\mathcal{Z}_1+\Theta_1^{11}(m),\Theta_2^{12}(m)=\Theta_1^{12}(m),$$
$$\Theta_2^{13}(m)=-m^2\mathcal{W}_1,\Theta_2^{22}(m)=\Theta_1^{22}(m)+m^2e^{-2\delta m}\mathcal{M}_{11},$$
$$\Theta_2^{23}(m)=m^2e^{-2\delta m}\mathcal{M}_{12}-m^2\mathcal{W}_2,\Theta_2^{33}(m)=m^2e^{-2\delta m}\mathcal{M}_{22},$$
$$\Theta_3^{11}(m)=\mathcal{U}_a+m\mathcal{Q}_1+m\{\mathcal{E}_1+\mathcal{E}_1^{\mathrm{T}}\},$$
$$\Theta_3^{12}(m)=-m\mathcal{Q}_1+m\mathcal{Q}_2^{\mathrm{T}}+m\{-\mathcal{E}_1+\mathcal{E}_2^{\mathrm{T}}\},$$
$$\Theta_3^{22}(m)=m\mathcal{Q}_1-m\{\mathcal{Q}_1+\mathcal{Q}_2^{\mathrm{T}}\}-m\{\mathcal{E}_1+\mathcal{E}_2^{\mathrm{T}}\},$$
$$\Theta_4^{11}(m)=\mathcal{U}_a+\Theta_3^{11}(m),\Theta_4^{12}(m)=\Theta_3^{12}(m),$$
$$\Theta_3^{13}(m)=-m^2\mathcal{E}_1,\Theta_4^{22}(m)=\Theta_3^{22}(m)+m^2e^{-2\delta m}\mathcal{N}_{11},$$
$$\Theta_4^{23}(m)=m^2e^{-2\delta m}\mathcal{N}_{12}-m^2\mathcal{E}_2,\Theta_4^{33}(m)=m^2e^{-2\delta m}\mathcal{N}_{22}.$$

Therefore, the LKFs $V(t)>0$. The proof follows directly from ref. [18], Proposition 1.

3.1 | Stability Analysis

Subsequently, the H_∞ performance of Equations (14) and (15) is examined by employing the LKFs in Equation (21), from which the main result is obtained.

Theorem 1. *Let the scalars $\delta>0$, and matrices $E>0$, $\mathcal{P}_1>0$, $\mathcal{P}_2=\mathcal{P}_2^{\mathrm{T}}>0$, $\mathcal{R}>0$, $\mathcal{S}_f>0$ with $\mathcal{S}_1=\mathcal{S}_1^{\mathrm{T}}$, $\mathcal{X}_k>0$, $\zeta_k>0$ for $f=1,2$, $k=1,2,3$ and define $\mathcal{P}>0$, $\mathcal{S}>0$. Given the control gain $\mathcal{K}_z$, observer gains $\mathcal{I}_j$, $\mathcal{L}_j$ and matrices $\mathcal{U}\in\mathbb{R}^{9n_\vartheta\times n_\vartheta}$, $\mathcal{H}\in\mathbb{R}^{10n_\vartheta\times n_\vartheta}$, $\mathcal{D}\in\mathbb{R}^{n_\vartheta\times n_\vartheta}$, $\mathcal{K}\in\mathbb{R}^{n_\vartheta\times n_\vartheta}$, the following LMIs are required to be satisfied:*

$$\Phi_{ra,\vartheta eij}(m_k)<0, r=1,2, m_k\in\{\varepsilon,m\},\tag{27}$$

where

$$\Phi_{1a,\vartheta eij}(m_k)=T_{1\vartheta eij}+m_kT_{2\vartheta e},$$

$$\Phi_{2a,\vartheta eij}(m_k)=\begin{bmatrix}T_{1a,\vartheta eij} & 0\\ * & 0\end{bmatrix}-m_kT_{3f,\vartheta e},$$

$$T_{1a,\vartheta ei}=\begin{bmatrix}\Xi_{1\vartheta ij}^{11} & \Xi_{1\vartheta,e}^{12}\\ * & \Xi_{1a,ej}^{22}\end{bmatrix},T_{2\vartheta e}=\begin{bmatrix}\Xi_{2\vartheta}^{11} & \Xi_2^{12}\\ * & \Xi_{2e}^{22}\end{bmatrix},$$

$$T_{3f,\vartheta e}=\begin{bmatrix}\Xi_{3\vartheta,e}^{11} & \Xi_3^{12} & \Xi_{3\vartheta}^{13} & \Xi_{3e}^{14}\\ * & \Xi_{3f}^{22} & \Xi_3^{23} & \Xi_3^{24}\\ * & * & \Xi_{3\vartheta}^{33} & \Xi_3^{34}\\ * & * & * & \Xi_{3e}^{44}\end{bmatrix},$$

$$\begin{aligned}\Xi_{1\vartheta i}^{11}=&e_1^{\mathrm{T}}\Pi_1e_1+e_4^{\mathrm{T}}\Pi_2e_4+e_3^{\mathrm{T}}\Pi_3e_3\\&+(l_2-l_1)(e_7^{\mathrm{T}}\zeta_3e_7+e_9^{\mathrm{T}}Ie_9)+\Omega_1-Y_1^{\mathrm{T}}\mathcal{R}_1Y_1\\&-\Omega_2-e^{-2\delta\bar{h}}(e_6^{\mathrm{T}}\mathcal{J}_1e_6+e_5^{\mathrm{T}}\mathcal{J}_2e_5+\Pi_4^{\mathrm{T}}\mathcal{J}_3\Pi_4)\\&+\wedge_1(\Omega_3+\Omega_4)-\frac{\pi^2}{4(l_2-l_1)^2}Y_4^{\mathrm{T}}\mathcal{D}Y_4\\&+e_1^{\mathrm{T}}\omega_3e_5+e_4^{\mathrm{T}}\omega_4e_1+e_4^{\mathrm{T}}\omega_5e_5-\Omega_5+\Omega_6\\&+e_8^{\mathrm{T}}C^{\mathrm{T}}ECe_8,\end{aligned}$$

$$\begin{aligned}\Xi_{1ej}^{22}=&\Omega_7+e_{10}^{\mathrm{T}}\Pi_5e_{10}+e_{12}^{\mathrm{T}}\Pi_6e_{12}-Y_5^{\mathrm{T}}\mathcal{Q}_1Y_5-\omega_8\\&-\mathrm{e}^{-2\delta\bar{h}}(e_{15}^{\mathrm{T}}\mathcal{H}_1e_{15}+e_{14}^{\mathrm{T}}\mathcal{H}_2e_{14}+\Pi_7^{\mathrm{T}}\mathcal{H}_3\Pi_7)\\&-(l_2-l_1)(\Omega_9+\Omega_{10})-\frac{\pi^2}{4(l_2-l_1)^2}Y_8^{\mathrm{T}}\mathcal{K}Y_8\\&-e_{10}^{\mathrm{T}}\omega_{10}e_{14}+\omega_{11}+\omega_{12}+e_{13}^{\mathrm{T}}\omega_{11}e_{10}\\&+e_{13}^{\mathrm{T}}\omega_{12}e_{14}-\omega_{13}-e_{13}^{\mathrm{T}}\omega_{13}e_{13}+\omega_{14}\\&+e_{18}^{\mathrm{T}}C^{\mathrm{T}}ECe_{18},\end{aligned}$$

$$\Xi_{1\vartheta,e}^{12}=-\wedge_1e_{18}^{\mathrm{T}}\mathcal{K}_z^{\mathrm{T}}\mathcal{B}^{\mathrm{T}}\mathcal{D}_q^{\mathrm{T}}\Upsilon^{\mathrm{T}}\Pi_8,$$

$$\begin{aligned}\Xi_{2\vartheta}^{11}=&\Omega_{15}+\Omega_{16}+2\delta Y_1^{\mathrm{T}}\mathcal{R}_1Y_1+2\delta\Omega_{17}+e_2^{\mathrm{T}}\mathcal{M}_{11}e_2\\&+\Omega_{18}+e_4^{\mathrm{T}}\mathcal{M}_{22}e_4,\end{aligned}$$

$$\begin{aligned}\Xi_{2e}^{22}=&\Omega_{19}+\Omega_{20}+2\delta Y_5^{\mathrm{T}}\mathcal{Q}_1Y_5+2\delta e_{11}^{\mathrm{T}}\mathcal{Q}_2Y_5\\&+e_{11}^{\mathrm{T}}\mathcal{N}_{11}e_{11}+\Omega_{21}+e_{13}^{\mathrm{T}}\mathcal{N}_{22}e_{13},\end{aligned}$$

$$\Xi_{3\vartheta e}^{11}=e^{-2\delta m}e_2^{\mathrm{T}}\mathcal{M}_{11}e_2+e^{-2\delta m}e_{11}^{\mathrm{T}}\mathcal{N}_{11}e_{11},$$
$$\Xi_{3\vartheta}^{13}=e^{-2\delta m}e_2^{\mathrm{T}}\mathcal{M}_{12}+\mathcal{W}_9^{\mathrm{T}}\mathcal{U},$$
$$\Xi_{3e}^{14}=e^{-2\delta m}e_{11}^{\mathrm{T}}\mathcal{N}_{12}+\mathcal{W}_{10}^{\mathrm{T}}\mathcal{H},$$
$$\Xi_{3f}^{22}=-E,\Xi_{3\vartheta}^{33}=e^{-2\delta m}\mathcal{M}_{22},\Xi_{3e}^{44}=e^{-2\delta m}\mathcal{N}_{22},$$
$$e_g=\left[0_{n\times(g-1)n}I_n0_{n\times(19-g)n}\right],g=19,$$
$$\mathcal{W}_9=\mathrm{col}\{e_1,e_2,...,e_i\},i=9,$$
$$\mathcal{W}_{10}=\mathrm{col}\{e_1,e_2,...,e_j\},j=19.$$

It follows that exponential stability is guaranteed for the fuzzy delayed DPSs in Equation (4) governed by the observer-based noncollocated ETSD controller Equation (12) as well as for the error system with random sensor faults under fuzzy BMs Equation (10). The detailed proof is provided in the Appendix A.

3.2 | Controller Design

Theorem 2. *For given scalars $\delta > 0$, r_1, r_2, d_1, d_2 and ϖ, there exist matrices $\overline{E} > 0$, $\overline{Z_1} > 0$, $\overline{\mathcal{R}}_1 = \overline{\mathcal{R}}_1^{\mathrm{T}}$, $\overline{\mathcal{R}}_2$, $\overline{\mathcal{W}}_f > 0$, $\overline{\mathcal{O}} > 0$, $\overline{\mathcal{E}}_f > 0$, $\overline{\mathcal{P}}_1$, $\overline{\mathcal{S}}_f$, $\overline{\mathcal{X}}_k$, $\overline{\mathcal{D}}$, $\overline{\mathcal{K}} > 0$, $f = 1, 2$, $k = 1, 2, 3$, $r_1\Upsilon\overline{W} = r_1\overline{W}^{\mathrm{T}}\Upsilon$, $r_2\Upsilon\overline{W} = r_2\overline{W}^{\mathrm{T}}\Upsilon$, $\overline{\mathcal{M}}$, $\overline{\mathcal{N}} \in \mathbb{R}^{2n_\vartheta \times 2n_\vartheta} > 0$, $\overline{\mathcal{I}}_j, \overline{\mathcal{L}}_j, \overline{\mathcal{K}}_z \in \mathbb{R}^{n_u \times n_\vartheta}$, $\overline{\mathcal{U}} \in \mathbb{R}^{9n_\vartheta \times n_\vartheta}$, $\overline{\mathcal{H}} \in \mathbb{R}^{10n_\vartheta \times n_\vartheta}$, the following LMIs hold:*

$$\overline{\Theta}_\iota(m) > 0, \iota = 1, 2, 3, 4, \tag{28}$$

$$\overline{\Phi}_{ra,\vartheta eij}(m_k) < 0, r = 1, 2, m_k \in \{\varepsilon, m\}, \tag{29}$$

where

$$\overline{\Theta}_1(m) = \begin{bmatrix} \overline{\Theta}_1^{11}(m) & \overline{\Theta}_1^{12}(m) \\ * & \overline{\Theta}_1^{22}(m) \end{bmatrix},$$

$$\overline{\Theta}_2(m) = \begin{bmatrix} \overline{\Theta}_2^{11}(m) & \overline{\Theta}_2^{12}(m) & \overline{\Theta}_2^{13}(m) \\ * & \overline{\Theta}_2^{22}(m) & \overline{\Theta}_2^{23}(m) \\ * & * & \overline{\Theta}_2^{33}(m) \end{bmatrix},$$

$$\overline{\Theta}_3(m) = \begin{bmatrix} \overline{\Theta}_3^{11}(m) & \overline{\Theta}_3^{12}(m) \\ * & \overline{\Theta}_3^{22}(m) \end{bmatrix},$$

$$\overline{\Theta}_4(m) = \begin{bmatrix} \overline{\Theta}_4^{11}(m) & \overline{\Theta}_4^{12}(m) & \overline{\Theta}_4^{13}(m) \\ * & \overline{\Theta}_4^{22}(m) & \overline{\Theta}_4^{23}(m) \\ * & * & \overline{\Theta}_4^{33}(m) \end{bmatrix},$$

$$\overline{\Theta}_1^{11}(m) = \overline{\mathcal{Z}}_1 + m\overline{\mathcal{R}}_1 + m\{\overline{\mathcal{W}}_1 + \overline{\mathcal{W}}_1^{\mathrm{T}}\},$$

$$\overline{\Theta}_1^{12}(m) = -m\overline{\mathcal{R}}_1 + m\overline{\mathcal{R}}_2^{\mathrm{T}} + m\{-\overline{\mathcal{W}}_1 + \overline{\mathcal{W}}_2^{\mathrm{T}}\},$$

$$\overline{\Theta}_1^{22}(m) = m\overline{\mathcal{R}}_1 - m\{\overline{\mathcal{R}}_1 + \overline{\mathcal{R}}_2^{\mathrm{T}}\} - m\{\overline{\mathcal{W}}_1 + \overline{\mathcal{W}}_2^{\mathrm{T}}\},$$

$$\overline{\Theta}_2^{11}(m) = \overline{\mathcal{Z}}_1 + \overline{\Theta}_1^{11}(m), \overline{\Theta}_2^{12}(m) = \overline{\Theta}_1^{12}(m),$$

$$\overline{\Theta}_2^{13}(m) = -m^2\overline{\mathcal{W}}_1, \overline{\Theta}_2^{22}(m) = \overline{\Theta}_1^{22}(m) + m^2e^{-2\delta m}\overline{\mathcal{M}}_{11},$$

$$\overline{\Theta}_2^{23}(m) = m^2e^{-2\delta m}\overline{\mathcal{M}}_{12} - m^2\overline{\mathcal{W}}_2\overline{\Theta}_2^{33}(m) = m^2e^{-2\delta m}\overline{\mathcal{M}}_{22},$$

$$\overline{\Theta}_3^{11}(m) = \overline{\mathcal{U}}_a + m\overline{\mathcal{Q}}_1 + m\{\overline{\mathcal{E}}_1 + \overline{\mathcal{E}}_1^{\mathrm{T}}\},$$

$$\overline{\Theta}_3^{12}(m) = -m\overline{\mathcal{Q}}_1 + m\overline{\mathcal{Q}}_2^{\mathrm{T}} + m\{-\overline{\mathcal{E}}_1 + \overline{\mathcal{E}}_2^{\mathrm{T}}\},$$

$$\overline{\Theta}_3^{22}(m) = m\overline{\mathcal{Q}}_1 - m\{\overline{\mathcal{Q}}_1 + \overline{\mathcal{Q}}_2^{\mathrm{T}}\} - m\{\overline{\mathcal{E}}_1 + \overline{\mathcal{E}}_2^{\mathrm{T}}\},$$

$$\overline{\Theta}_4^{11}(m) = \overline{\mathcal{U}}_a + \overline{\Theta}_3^{11}(m), \overline{\Theta}_4^{12}(m) = \overline{\Theta}_3^{12}(m),$$

$$\overline{\Theta}_3^{13}(m) = -m^2\overline{\mathcal{E}}_1, \overline{\Theta}_4^{22}(m) = \overline{\Theta}_3^{22}(m) + m^2e^{-2\delta m}\overline{\mathcal{N}}_{11},$$

$$\overline{\Theta}_4^{23}(m) = m^2e^{-2\delta m}\overline{\mathcal{N}}_{12} - m^2\overline{\mathcal{E}}_2, \overline{\Theta}_4^{33}(m) = m^2e^{-2\delta m}\overline{\mathcal{N}}_{22},$$

$$\overline{\Phi}_{1a,\vartheta eij}(m_k) = \overline{T}_{1\vartheta eij} + m_k\overline{T}_{2\vartheta e}$$

$$\overline{\Phi}_{2a,\vartheta eij}(m_k) = \begin{bmatrix} \overline{T}_{1a,\vartheta ij} & 0 \\ * & 0 \end{bmatrix} - m_k\overline{T}_{3f,\vartheta e}$$

$$\overline{T}_{1a,\vartheta ei} = \begin{bmatrix} \overline{\Xi}_{1\vartheta ij}^{11} & \overline{\Xi}_{1\vartheta,e}^{12} \\ * & \overline{\Xi}_{1a,ej}^{22} \end{bmatrix},$$

$$\overline{T}_{2\vartheta e} = \begin{bmatrix} \overline{\Xi}_{2\vartheta}^{11} & \overline{\Xi}_2^{12} \\ * & \overline{\Xi}_{2e}^{22} \end{bmatrix},$$

$$\overline{T}_{3f,\vartheta e} = \begin{bmatrix} \overline{\Xi}_{3\vartheta,e}^{11} & \overline{\Xi}_3^{12} & \overline{\Xi}_{3\vartheta}^{13} & \overline{\Xi}_{3e}^{14} \\ * & \overline{\Xi}_{3f}^{22} & \overline{\Xi}_3^{23} & \overline{\Xi}_3^{24} \\ * & * & \overline{\Xi}_{3\vartheta}^{33} & \overline{\Xi}_3^{34} \\ * & * & * & \overline{\Xi}_{3e}^{44} \end{bmatrix},$$

$$\begin{aligned}\overline{\Xi}_{1\vartheta i}^{11} &= e_1^{\mathrm{T}}\overline{\Pi}e_1 + e_4^{\mathrm{T}}\overline{\Pi}e_4 - (l_2 - l_1)\left(e_7^{\mathrm{T}}\overline{\zeta}_3e_7 + \wedge_2\right) + \overline{\Omega}_1 \\ &\quad + e_3^{\mathrm{T}}\overline{\Pi}_3e_3 - Y_1^{\mathrm{T}}\overline{\mathcal{R}}_1Y_1 - \overline{\Omega}_2 \\ &\quad - e^{-2\delta\overline{h}}\left(e_6^{\mathrm{T}}\overline{\mathcal{J}}_1e_6 + e_5^{\mathrm{T}}\overline{\mathcal{J}}_2e_5 + \Pi_4^{\mathrm{T}}\overline{\mathcal{J}}_3\Pi_4\right) \\ &\quad + d_1\wedge_1\overline{\Omega}_3 + r_1\wedge_1\overline{\Omega}_4 - \frac{\pi^2}{4(l_2 - l_1)^2}Y_4^{\mathrm{T}}\overline{\mathcal{D}}Y_4 \\ &\quad + d_1e_1^{\mathrm{T}}\overline{\omega}_3e_5 + r_1e_4^{\mathrm{T}}\overline{\omega}_2e_1 + r_1e_4^{\mathrm{T}}\overline{\omega}_3e_5 - \overline{\Omega}_5 + \overline{\Omega}_6 \\ &\quad + e_8^{\mathrm{T}}C^{\mathrm{T}}\overline{E}Ce_8,\end{aligned}$$

$$\begin{aligned}\overline{\Pi}_{1ej}^{22} &= \overline{\Omega}_7 + e_{10}^{\mathrm{T}}\overline{\Pi}_5e_{10} + e_{12}^{\mathrm{T}}\overline{\Pi}_6e_{12} - Y_5^{\mathrm{T}}\overline{\mathcal{Q}}_1Y_5 - \overline{\Omega}_8 \\ &\quad - \mathrm{e}^{-2\delta\overline{h}}\left(e_{15}^{\mathrm{T}}\overline{\mathcal{H}}_1e_{15}e_{14}^{\mathrm{T}}\overline{\mathcal{H}}_2e_{14} + \overline{\Pi}_7^{\mathrm{T}}\overline{\mathcal{H}}_3\overline{\Pi}_7\right) \\ &\quad - d_2(l_2 - l_1)\overline{\Omega}_9 - r_2(l_2 - l_1)\overline{\Omega}_{10} \\ &\quad - \frac{\pi^2}{4(l_2 - l_1)^2}Y_8^{\mathrm{T}}\mathcal{K}Y_8 + d_2e_{10}^{\mathrm{T}}\overline{\omega}_6e_{14} + \overline{\Omega}_{11} + \overline{\Omega}_{12} \\ &\quad + r_2e_{13}^{\mathrm{T}}\overline{\omega}_5e_{10} + r_2e_{13}^{\mathrm{T}}\overline{\omega}_6e_{14} - \overline{\Omega}_{13} - r_2e_{13}^{\mathrm{T}}\overline{\omega}_4e_{13} \\ &\quad + \overline{\Omega}_{14} + e_{18}^{\mathrm{T}}C^{\mathrm{T}}\overline{E}Ce_{18},\end{aligned}$$

$$\begin{aligned}\overline{\Xi}_{1\vartheta,e}^{12} &= -d_1\wedge_1e_{18}^{\mathrm{T}}\mathcal{K}_z^{\mathrm{T}}\mathcal{B}^{\mathrm{T}}\mathcal{D}_q^{\mathrm{T}}\Upsilon^{\mathrm{T}}e_7 \\ &\quad - r_1\wedge_1e_{18}^{\mathrm{T}}\mathcal{K}_z^{\mathrm{T}}\mathcal{B}^{\mathrm{T}}\mathcal{D}_q^{\mathrm{T}}\Upsilon e_4 + d_2e_1^{\mathrm{T}}\overline{\Pi}_7e_{10} \\ &\quad + r_2e_1^{\mathrm{T}}\overline{\Pi}_8e_{13},\end{aligned}$$

$$\overline{\Xi}_{1\vartheta,e}^{13} = d_1e_1^{\mathrm{T}}\overline{\Pi}_9^{\mathrm{T}}\overline{\mathcal{V}}^{\mathrm{T}}\mathcal{F}_i, \overline{\Xi}_{1\vartheta,e}^{33} = -\gamma^2\mathcal{I},$$

$$\begin{aligned}\overline{\Xi}_{2\vartheta}^{11} &= \overline{\Omega}_{15} + \overline{\Omega}_{16} + 2\delta Y_1^{\mathrm{T}}\overline{\mathcal{R}}_1Y_1 + 2\delta\overline{\Omega}_{17} + e_2^{\mathrm{T}}\mathcal{M}_{11}e_2 \\ &\quad + \overline{\Omega}_{18} + e_4^{\mathrm{T}}\overline{\mathcal{M}}_{22}e_4,\end{aligned}$$

$$\begin{aligned}\overline{\Xi}_{2e}^{22} &= \overline{\Omega}_{19} + \overline{\Omega}_{20} + 2\delta Y_5^{\mathrm{T}}\overline{\mathcal{Q}}_1Y_5 + 2\delta e_{11}^{\mathrm{T}}\overline{\mathcal{Q}}_2Y_5 \\ &\quad + e_{11}^{\mathrm{T}}\overline{\mathcal{N}}_{11}e_{11} + \overline{\Omega}_{21} + e_{13}^{\mathrm{T}}\overline{\mathcal{N}}_{22}e_{13},\end{aligned}$$

$$\overline{\Xi}_{3\vartheta e}^{11} = e^{-2\delta m}e_2^{\mathrm{T}}\overline{\mathcal{M}}_{11}e_2 + e^{-2\delta m}e_{11}^{\mathrm{T}}\overline{\mathcal{N}}_{11}e_{11},$$

$$\overline{\Xi}_{3\vartheta}^{13} = e^{-2\delta m}e_2^{\mathrm{T}}\overline{\mathcal{M}}_{12} + \mathcal{W}_9^{\mathrm{T}}\overline{\mathcal{U}},$$

$$\overline{\Xi}_{3e}^{14} = e^{-2\delta m}e_{11}^{\mathrm{T}}\overline{\mathcal{N}}_{12} + \mathcal{W}_{10}^{\mathrm{T}}\overline{\mathcal{H}},$$

$$\overline{\Xi}_{3f}^{22} = -\overline{E}, \overline{\Xi}_{3\vartheta}^{33} = e^{-2\delta m}\overline{\mathcal{M}}_{22}, \overline{\Xi}_{3e}^{44} = e^{-2\delta m}\overline{\mathcal{N}}_{22},$$

$$
\begin{aligned}
e_g &= \left[0_{n\times(g-1)n} I_n 0_{n\times(19-g)n}\right], g = 19,\\
\mathcal{W}_9 &= \mathrm{col}\{e_1, e_2, ..., e_i\}, i = 9,\\
\mathcal{W}_{10} &= \mathrm{col}\{e_1, e_2, ..., e_j\}, j = 19.
\end{aligned} \tag{30}
$$

Based on the solution to the LMIs in Theorem 2, the gain matrices of the observer and the boundary controller can be explicitly derived as follows:

$$
\mathcal{I}_j = \overline{I}_j \overline{\mathcal{V}}^{-1}, \mathcal{L}_j = \overline{L}_j \overline{\mathcal{V}}^{-1}, \mathcal{K}_z = \overline{K}_z \overline{\mathcal{V}}^{-1}, j, z \in \mathbb{M}. \tag{31}
$$

Proof. Denote $\overline{\mathcal{P}}_1 \triangleq \overline{\mathcal{V}}^{\mathrm{T}} \mathcal{P}_1 \overline{\mathcal{V}}$, $\overline{\mathcal{X}}_k \triangleq \overline{\mathcal{V}}^{\mathrm{T}} \mathcal{X}_k \overline{\mathcal{V}}$, $\overline{\mathcal{S}}_f \triangleq \overline{\mathcal{V}}^{\mathrm{T}} \mathcal{S}_f \overline{\mathcal{V}}$, $f = 1, 2$, $k = 1, 2, 3$, $\overline{\mathcal{R}} \triangleq \overline{\mathcal{V}}^{\mathrm{T}} \mathcal{R} \overline{\mathcal{V}}$, $\overline{\mathcal{D}} \triangleq \overline{\mathcal{V}}^{\mathrm{T}} \mathcal{D} \overline{\mathcal{V}}$, $\overline{\mathcal{K}} \triangleq \overline{\mathcal{V}}^{\mathrm{T}} \mathcal{K} \overline{\mathcal{V}}$, $\mathcal{Z}_2 \triangleq r_1 \overline{\mathcal{V}}^{-1}$, $\mathcal{U}_2 \triangleq r_2 \overline{\mathcal{V}}^{-1}$, $\mathcal{P} \triangleq d_1 \overline{\mathcal{V}}^{-1}$, $\mathcal{S} \triangleq d_2 \overline{\mathcal{V}}^{-1}$, $\overline{\mathcal{U}} \triangleq \overline{\mathcal{W}} \mathcal{U} \overline{\mathcal{V}}$ and $\overline{\mathcal{W}} \triangleq \mathrm{diag}\left\{\underbrace{\overline{\mathcal{V}}, ..., \overline{\mathcal{V}}}_{7}, \overline{\mathcal{V}}, \overline{\mathcal{V}}\right\}$.

For a scalar $\varpi > 0$, the inequality holds as follows:

$$
\overline{\mathcal{V}}^{\mathrm{T}} \overline{\mathcal{V}} \geq \varpi\left(\overline{\mathcal{V}} + \overline{\mathcal{V}}^{\mathrm{T}}\right) - \varpi^2 I.
$$

Applying a congruence transformation with $\wedge^{\mathrm{T}}$ and $\wedge$ to Equation (27) and employing the Schur complement yields Equation (29).

Remark 8. Theorem 2 provides the LMI-based sufficient conditions for the proposed fuzzy NBSDC design. By counting the decision matrices involved in the LKFs and the slack-variable construction, the LMIs Equations (28) and (29) contain 19 symmetric matrices and 2 general matrices of size $n_\vartheta \times n_\vartheta$, together with m boundary feedback gain matrices $K_z \in \mathbb{R}^{n_u \times n_\vartheta}$ associated with the fuzzy rules. Therefore, the total number of scalar decision variables can be calculated as $N_{\mathrm{dec}} = \frac{47n_\vartheta^2 + 19n_\vartheta}{2} + mn_\vartheta n_u$.

Clearly, the computational burden of solving LMIs Equations (28) and (29) grows quadratically with the state dimension n_ϑ and linearly with the product $n_\vartheta n_u$, and it also increases with the fuzzy rule number m.

4 | Numerical Illustration

An example is provided to verify the effectiveness of the designed control scheme.

Example: Consider the tumour cell diffusion model from ref. [36] and its T–S fuzzy parabolic representation used for control design from ref. [17]. The nonlinearity mainly comes from the cubic reaction term $-\vartheta_1^3(r, t)$, whereas the time-varying delay $\tau(t)$ complicates the spatiotemporal evolution. They are described by the following nonlinear DPSs:

$$
\begin{cases}
\vartheta_{1,t}(r, t) = \vartheta_{1,rr}(r, t) + \vartheta_1(r, t) - \vartheta_1^3(r, t)\\
\qquad\qquad - 0.5\vartheta_1(r, t - \tau_1(t)) - \vartheta_2(r, t)\\
\qquad\qquad + \omega(r, t),\\
\vartheta_{2,t}(r, t) = \beta\vartheta_{2,rr}(r, t) + \omega\vartheta_1(r, t) + \eta\vartheta_2(r, t)\\
\qquad\qquad - 0.1\vartheta_2(r, t - \tau_1(t)),\\
\vartheta_{r,r}(0, t) = 0, r = 1, 2,\\
\vartheta_{1,r}(1, t) = u(t),\ \vartheta_{2,r}(1, t) = 0,\\
\vartheta_{1,0}(r) = 0.1\cos(\pi r/5),\\
\vartheta_{2,0}(r) = 0.05\cos(\pi r/5) + 0.02\sin(\pi r/2).
\end{cases} \tag{32}
$$

Select $\vartheta(r, t) \triangleq [\vartheta_1(r, t) \quad \vartheta_2(r, t)]^{\mathrm{T}}$. In accordance with the form of Equation (1), the parameters of Equation (32) are given by

$$
\Upsilon = \begin{bmatrix} 1 & 0 \\ 0 & \beta \end{bmatrix}, f(\vartheta(r, t)) = \begin{bmatrix} 1 - \vartheta_1^2(r, t) & -1 \\ \omega & -\eta \end{bmatrix} \vartheta(r, t),
$$
$$
g_1(\vartheta(r, t - \tau_1(t))) = \begin{bmatrix} -0.5 & 0 \\ 0 & -0.1 \end{bmatrix} \vartheta(r, t - \tau_1(t)).
$$

Moreover, we set the premise variable as $\delta(r, t) = \vartheta(r, t)$, with the specific choice $\delta(r, t) = \vartheta_1^2(r, t)$, where $\vartheta_1(r, t) \in [-\overline{\rho}, \overline{\rho}]$ and $\overline{\rho} = 1.5$, which leads to

$$
\delta(r, t) = \theta_2(\delta(r, t)) \cdot 0 + \theta_1(\delta(r, t)) \cdot \overline{\rho}^2, \tag{33}
$$

and

$$
\sum_{\ell=1}^{2} \theta_\ell(\delta(r, t)) = 1, \theta_\ell(\delta(r, t)) \geqslant 0. \tag{34}
$$

From Equations (33) and (34), the corresponding membership functions can be obtained:

$$
\theta_1(\delta(r, t)) \triangleq \frac{\delta(r, t)}{\overline{\rho}^2}, \theta_2(\delta(r, t)) \triangleq 1 - \theta_1(\delta(r, t)). \tag{35}
$$

Thus, the fuzzy delayed DPSs are derived as follows:

$$
\begin{aligned}
\vartheta_t(r, t) =& \{\Upsilon\vartheta_r(r, t)\}_r + \sum_{i=1}^{2} \mathcal{W}_i(\delta(r, t)) \times \{\mathcal{A}_i\vartheta(r, t)\\
&+ \mathcal{A}_{di}\vartheta(r, t - \tau(t)) + \mathcal{F}_i\omega(r, t)\},
\end{aligned} \tag{36}
$$

where $\theta_i(\delta(r, t)) = \mathcal{W}_i(\delta(r, t))$ and $\tau(t) = 0.5 + 0.2\sin(t)$.

$$
A_1 = \begin{bmatrix} 1 & -1 \\ 0.45 & -0.1 \end{bmatrix}, A_2 = \begin{bmatrix} 1 - \overline{\rho}^2 & -1 - \overline{\rho}^2 \\ 0.45 & -0.1 \end{bmatrix},
$$
$$
A_{d1} = \begin{bmatrix} -1.25 & -1 \\ 0.45 & -0.1 \end{bmatrix}, A_{d2} = \begin{bmatrix} -1.25 - \overline{\rho}^2 & -1 \\ 0.45 & -0.1 \end{bmatrix},
$$
$$
F_1 = \begin{bmatrix} -0.5 & 0 \\ 0 & -0.5 \end{bmatrix}, F_2 = F_1, \beta = 1, \omega = 1, \eta = -1.
$$

Select $\bar{\tau} = 0.5$, $r_1 = 0.1$ and $r_2 = 0.2$. Select $\zeta_1 = 6I_2$, $\zeta_2 = 3I_2$, $\zeta_3 = 6I_2$, $d_1 = 0.9001$, $d_2 = 0.5975$, $\delta = 0.1$ and $\varpi = 0.2207$. Assuming a 20% reduction in actuator signal strength. Consider $\mathcal{S} \triangleq \{1, 2\}$, $\mathcal{D}_1 = 1$ and $\mathcal{D}_2 = 0.8$. The deception attack is modelled by

$$f\left(\hat{h}_{l_2}(t_k)\right) = \left[\tanh\left(\sqrt{\frac{0.1^2}{12}}\hat{h}_{l_2}(t_k)\right) \quad \tanh\left(\sqrt{\frac{0.1^2}{12}}\hat{h}_{l_2}(t_k)\right)\right],$$

and the conditions in Equation (13) hold with $C = \text{diag}\{0.1, 0.2\}$. The actuator failure transition rate matrix is expected to be

$$\Pi = \begin{bmatrix} -0.1 & 0.8 \\ 0.1 & -0.8 \end{bmatrix}.$$

For $\gamma = 0.2678$, a suboptimal solution is obtained by solving the SDP consisting of the four positive-definite LMIs in Equation (28) and the four negative-definite LMIs in Equation (29) (8 coupled LMIs in total), and the resulting observer gains in Equation (18) together with the boundary controller gains in Equation (16) are given by:

$$\begin{aligned} \mathcal{I}_j &= 10^4 \times \begin{bmatrix} -5.9986 & -3.5296 \\ -5.3777 & -3.7158 \end{bmatrix}, \\ \mathcal{L}_j &= 10^4 \times \begin{bmatrix} 5.2989 & 3.6266 \\ 7.4760 & 4.8219 \end{bmatrix}, \\ \mathcal{K}_z &= \begin{bmatrix} 134.1587 & 76.6744 \\ 24.9742 & 15.1842 \end{bmatrix}. \end{aligned} \tag{37}$$

The external disturbance is chosen to be

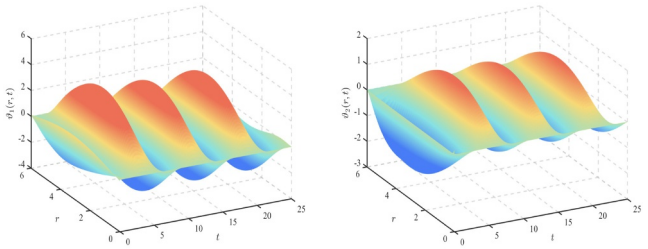
$$\omega(r, t) = (1 + 2r)\mathrm{e}^{-1.5t}. \tag{38}$$

For the above settings, the controller parameters are determined from explicit design specifications rather than ad-hoc tuning. The target H_∞ attenuation level γ and the required convergence rate are first prescribed. Then, Q_1, Q_2 and R are chosen to emphasise boundary-state regulation whilst limiting control effort. With these settings, the LMIs in Equations (28) and (29) are solved using a standard convex optimisation solver and a feasible solution yielding a smaller H_∞ bound is adopted. The AETM threshold and scaling coefficients are selected within the LMI-admissible ranges to guarantee a reasonable minimum interevent time and are slightly adjusted to balance communication rate and transient performance. The simulation values of γ, Q_1, Q_2, R and the triggering coefficients follow this procedure.

At present, Figure 2 illustrates the open-loop spatiotemporal evolution of the tumour cell diffusion model without boundary regulation. Specifically, Figure 2a shows the spatiotemporal evolution of $\vartheta_1(r, t)$, whereas Figure 2b presents the corresponding evolution of $\vartheta_2(r, t)$. The results indicate that the two state variables exhibit oscillatory growth patterns driven by nonlinear dynamics, intrinsic delays and diffusion effects. In the absence of control, the amplitudes continue to fluctuate and gradually diverge, which reflects the uncontrolled spread of tumour cells. This observation demonstrates the necessity of introducing robust observation and regulation strategies for such DPSs. The observed divergent and oscillatory behaviours are mainly induced by the nonlinear reaction terms and delayed feedback, which cannot be stabilised by linear boundary control schemes.

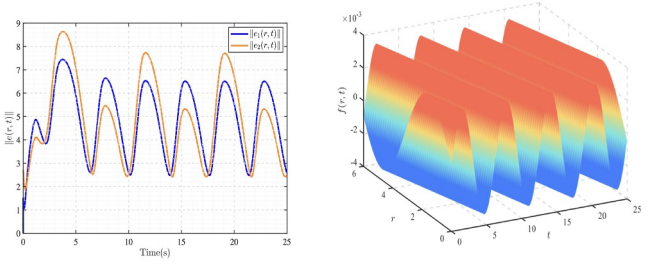
Figure 3a reveals the time evolution of the spatial $\mathcal{L}_2$ norm of the state-estimation error $e_i(r, t) = \vartheta_i(r, t) - \hat{\vartheta}_i(r, t)$ for $i = 1, 2$. The use of the $\mathcal{L}_2$ norm facilitates a more intuitive evaluation of the overall energy distribution and accumulation trend of the estimation deviations. The figure shows that the error trajectories display pronounced periodic oscillations with amplitudes that grow over time. This occurs in the absence of observer and controller intervention. The result indicates that the system is highly sensitive to disturbances and attacks, which makes accurate state estimation difficult. Figure 3b depicts the spatiotemporal evolution of the deception attack signal $f\left(\hat{h}_{l_2}(t_k)\right)$. It shows periodic spatial distribution and distinct temporal fluctuation characteristics, further exacerbating system uncertainty and instability.

Then, the fuzzy PDE observer in Equation (18) together with the ETSD controller in Equation (16), where the gains are chosen from Equation (37), is implemented on the nonlinear delayed parabolic DPS in Equation (25). The system is initialised with $\vartheta_{1,0}(r) = 0.1\cos(\pi r/5)$ and $\vartheta_{2,0}(r) = 0.05\cos(\pi r/5) + 0.02\sin(\pi r/2)$. The corresponding closed-loop trajectories of $\vartheta_1(\cdot, t)$



(a) (b)

FIGURE 2 | Open-loop trajectory of $\vartheta_1(\cdot, t)$ and $\vartheta_2(\cdot, t)$.



(a) (b)

FIGURE 3 | Open-loop trajectory of $\|e_i(\cdot, t)\|_2, i = 1, 2$ (a) and deception attack signal $f\left(\hat{h}_{l_2}(t_k)\right)$ (b).

and $\vartheta_2(\cdot, t)$ are illustrated in Figure 4. These results indicate that the proposed fuzzy observer-based ETSD control strategy achieves effective stabilisation and delivers satisfactory spatiotemporal regulation. In particular, the controller maintains robustness against time-varying delays, external disturbances and deception attacks, highlighting its practical relevance for networked DPSs.

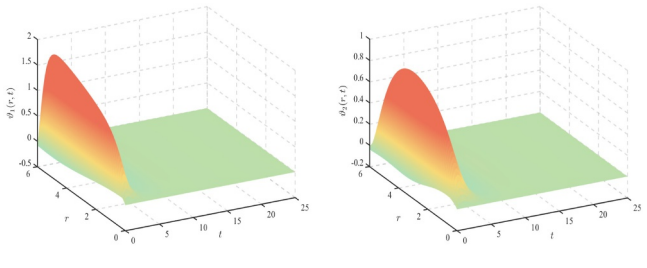
The time evolution of the state-estimation errors $e_1(r, t)$ and $e_2(r, t)$ is illustrated in Figure 5, where both DoS blocking and deception attacks are considered jointly. The pink shaded areas represent DoS intervals, during which communication is interrupted, whereas red square markers indicate the time instants of injected false data due to deception attacks. In both subplots, the estimation errors initially fluctuate significantly due to hybrid disturbances, but gradually stabilise over time. These results indicate that the T–S fuzzy modelling framework effectively captures the nonlinear dynamics across different operating regions, enabling the proposed observer-based ETSD controller to maintain stability under nonlinear, delayed and attack-prone conditions.

Each subplot includes two insets for detailed visualisation. The upper-left inset highlights the impact of frequent deception attacks in the early stage $t \in [0\,\text{s},\ 5\,\text{s}]$, where sharp deviations in estimation errors are evident. The lower-right inset focuses on the period $t \in [10\,\text{s},\ 20\,\text{s}]$ under sustained DoS attacks, revealing persistent but bounded estimation inaccuracies caused by delayed information updates. These results demonstrate that the proposed observer design remains resilient to inconsistent attack modes and sustains acceptable estimation accuracy under practical networked conditions. The bounded evolution of the spatial L_2 norms of $e_1(\cdot, t)$ and $e_2(\cdot, t)$ under disturbances and hybrid attacks confirms that the closed-loop error system satisfies the prescribed H_∞ performance level in Equation (20) with $\gamma = 0.2678$.

Figure 6 illustrates the trajectory of the control input $u(r, t)$ under hybrid attack scenarios. The evolution takes place under Markovian switching, with colour-coded segments denoting different operational modes. Red square markers highlight deception events, whereas pink-shaded regions indicate DoS intervals. The lower-right inset shows the Markov mode $r(t)$ as a piecewise-constant signal, so that each colour segment of $u(r, t)$ can be associated with a specific actuator condition. The upper-left and lower-left insets magnify typical responses during deception and DoS phases.

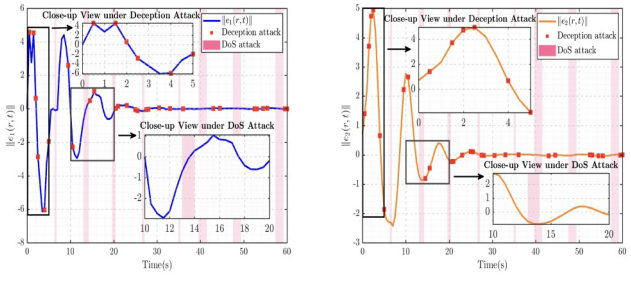
Figure 7 depicts the nonperiodic DoS attack sequence, where the pink stair-step curve serves as a binary transmission availability indicator: higher levels correspond to accessible communication and lower levels to blocked transmissions. The irregular timing and varying durations of these blocking intervals reproduce the aperiodic nature of realistic DoS disruptions, underscoring the practical relevance of the adopted attack model for networked control environments.

Finally, Figure 8a,b provide a comparison between two event-triggered mechanisms with distinct threshold formulations. The conventional ETM in Figure 8a operates with a fixed threshold σ, which under disturbance conditions leads to dense and irregular triggering intervals. This irregularity not only increases communication demand but also reflects limited adaptability to time-varying system dynamics. In contrast, the adaptive ETM in Figure 8b employs a dynamic threshold $\sigma(t)$ as defined in Equation (6), which evolves in accordance with the



(a) (b)

FIGURE 4 | Closed-loop trajectory of $\vartheta_1(\cdot, t)$ and $\vartheta_2(\cdot, t)$.



(a) (b)

FIGURE 5 | Closed-loop trajectory of $\|e_1(\cdot, t)\|_2$ and $\|e_2(\cdot, t)\|_2$ with hybrid attacks.

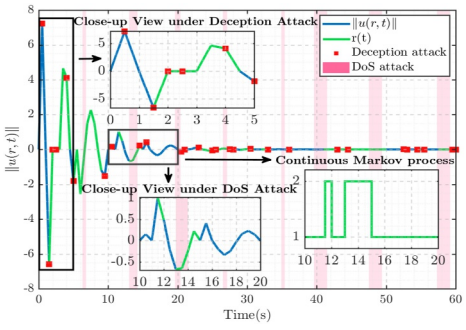


FIGURE 6 | Trajectory of $u(r, t)$ with hybrid attacks.

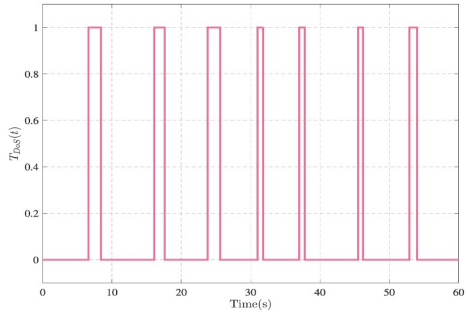


FIGURE 7 | Nonperiodic DoS attack.

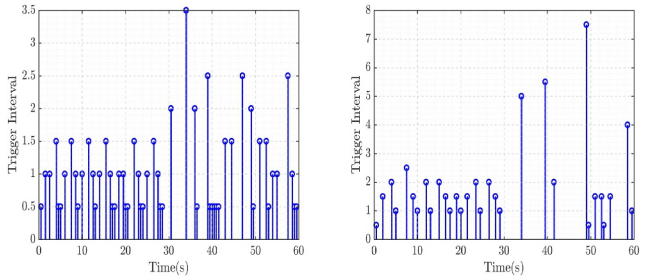


FIGURE 8 | ETM instants (a) and AETM instants (b).

instantaneous error trajectory. The resulting trigger sequence shows a more structured distribution with extended intervals and reduced frequency. In both subplots, the vertical impulses indicate the event-triggered update instants of the observer and controller, and denser clusters correspond to higher transmission rates. This pattern reflects a balance between error responsiveness and communication efficiency. Such behaviour highlights the ability of the adaptive strategy to significantly alleviate transmission burden while safeguarding closed-loop performance in networked control settings.

Simulation results indicate that the system in Equation (17), affected by stochastic sensor malfunctions and hybrid attacks, achieves stochastic exponential stability and ensures the desired H_∞ performance when regulated by the observer-based fuzzy noncollocated ETSD controller Equation (16).

5 | Conclusion

This paper proposed a boundary control method for nonlinear DPSs with limited BMs, aiming to improve state estimation accuracy and control performance under cyber-physical threats. An improved PDE-based boundary sampled-data observer with an AETM was developed to reduce communication overhead while maintaining estimation accuracy. A T–S fuzzy NBSDC was designed to address observation-actuation mismatch under partial state observability. The controller was further extended to hybrid attack scenarios, where inconsistent modes, such as DoS interruptions and deceptive signal injections, were modelled as a random process with energy-constrained deception signals. A Markov jump process was introduced to describe stochastic controller failures, enabling dynamic mode switching and improving fault tolerance. Stability conditions were derived using LKFs and LMIs, ensuring system stability and estimation error convergence. Simulation results on a tumour cell diffusion model verified the feasibility and effectiveness of the proposed method. Future work will extend the approach to coupled reaction-diffusion systems with mixed delays and network attacks and will also investigate real-time implementation and additional sensor-failure scenarios.

Funding

This work was supported by the Sichuan Science and Technology Program (Grants 25NSFSC2581 and 2024NSFSC2056), the National Natural Science Foundation of China (Grants 62402129, 62272119, 62372126, 62372129, U2436208 and U2468204), the Guangdong S&T Program (Grant 2024B0101010002), the Guangdong Basic and Applied Basic Research Foundation (Grants 2026A1515010143, 2020A1515010450 and 2021A1515012307) and Guangdong Key Laboratory of Industrial Control System Security Project (Grant 2024B1212020010).

Conflicts of Interest

The authors declare no conflicts of interest.

Data Availability Statement

The data that support the findings of this study are available from the corresponding author upon reasonable request. No real experimental datasets were generated or analysed; all results are based on simulation models described in the manuscript.

References

1. N. Bu, Y. Zhang, X. Li, W. Chen, and C. Jiang, "Passive Robust Control for Uncertain Hamiltonian Systems by Using Operator Theory," *CAAI Transactions on Intelligence Technology* 7, no. 4 (2022): 594–605, https://doi.org/10.1049/cit2.12142.

2. Y.-S. Wei, J.-F. Wang, J.-X. Wang, Q.-Y. Xu, and J. Lloret, "Iteration Dependent Interval Based Open-Closed-Loop Iterative Learning Control for Time Varying Systems With Vector Relative Degree," *CAAI Transactions on Intelligence Technology* 8, no. 3 (2023): 645–660, https://doi.org/10.1049/cit2.12213.

3. J. Wang and M. Krstic, "Event-Triggered Adaptive Control of a Parabolic PDE–ODE Cascade With Piecewise-Constant Inputs and Identification," *IEEE Transactions on Automatic Control* 68, no. 9 (2022): 5493–5508, https://doi.org/10.1109/tac.2022.3227916.

4. X. Xu and B. Li, "Semi-Global Stabilization of Parabolic PDE–ODE Systems With Input Saturation," *Automatica* 171 (2025): 111931, https://doi.org/10.1016/j.automatica.2024.111931.

5. Z. Zeng, C. Zhu, and S. M. Goetz, "Fault-Tolerant Multiparallel Three-Phase Two-Level Converters With Adaptive Hardware Reconfiguration," *IEEE Transactions on Power Electronics* 39, no. 4 (2024): 3925–3930, https://doi.org/10.1109/tpel.2024.3350186.

6. X. Xu and B. Li, "Pde-Based Observation and Predictor-Based Control for Linear Systems With Distributed Infinite Input and Output Delays," *Automatica* 170 (2024): 111845, https://doi.org/10.1016/j.automatica.2024.111845.

7. J. Wang, Y. Wu, C. P. Chen, Z. Liu, and W. Wu, "Adaptive Pi Event-Triggered Control for Mimo Nonlinear Systems With Input Delay," *Information Sciences* 677 (2024): 120817, https://doi.org/10.1016/j.ins.2024.120817.

8. T. Li, H. Shi, X. Bai, N. Li, and K. Zhang, "Rolling Bearing Performance Assessment With Degradation Twin Modeling Considering Interdependent Fault Evolution," *Mechanical Systems and Signal Processing* 224 (2025): 112194, https://doi.org/10.1016/j.ymssp.2024.112194.

9. X. Ju, Y. Jiang, L. Jing, and P. Liu, "Quantized Predefined-Time Control for Heavy-Lift Launch Vehicles Under Actuator Faults and Rate Gyro Malfunctions," *ISA Transactions* 138 (2023): 133–150, https://doi.org/10.1016/j.isatra.2023.02.022.

10. F. Ding, Z. Liu, Y. Wang, et al., "Intelligent Event Triggered Lane Keeping Security Control for Autonomous Vehicle Under Dos Attacks," *IEEE Transactions on Fuzzy Systems* 33 (2025): 3595–3607, https://doi.org/10.1109/TFUZZ.2025.3597276.

11. Z. Zhou, Y. Wang, G. Zhou, K. Nam, Z. Ji, and C. Yin, "A Twisted Gaussian Risk Model Considering Target Vehicle Longitudinal-Lateral Motion States for Host Vehicle Trajectory Planning," *IEEE Transactions on Intelligent Transportation Systems* 24, no. 12 (2023): 13685–13697, https://doi.org/10.1109/tits.2023.3298110.

12. R.-E. Precup, A.-T. Nguyen, and S. Blažič, "A Survey on Fuzzy Control for Mechatronics Applications," *International Journal of Systems Science* 55, no. 4 (2024): 771–813, https://doi.org/10.1080/00207721.2023.2293486.

13. X. Cai, K. Shi, Y. Sun, J. Cao, S. Wen, and Z. Tian, "Intelligent Event-Triggered Control Supervised by Mini-Batch Machine Learning and Data Compression Mechanism for Ts Fuzzy Ncss Under Dos Attacks," *IEEE Transactions on Fuzzy Systems* 32, no. 3 (2023): 804–815, https://doi.org/10.1109/tfuzz.2023.3308933.

14. A. Baihan, E. Ghith, H. Garg, et al., "A Hybrid Meta-Heuristic Algorithm for Optimum Micro-Robotic Position Control With Pid Controller," *International Journal of Computational Intelligence Systems* 18, no. 1 (2025): 86, https://doi.org/10.1007/s44196-025-00799-3.

15. D. He, H. Wang, Y. Tian, and R.-E. Precup, "Model-Free Global Sliding Mode Control Using Adaptive Fuzzy System Under Constrained Input Amplitude and Rate for Mechatronic Systems Subject to Mismatched Disturbances," *Information Sciences* 697 (2025): 121769, https://doi.org/10.1016/j.ins.2024.121769.

16. Y. Xia, J. He, H.-K. Lam, L. Rutkowski, and R.-E. Precup, "Non-Fragile Fuzzy Control of Input-Saturated Systems With Global Prescribed Performance via an Error-Triggered Mechanism," *Information Sciences* 711 (2025): 122111, https://doi.org/10.1016/j.ins.2025.122111.

17. Y. Li, K. Shi, S. Wang, et al., "Fuzzy Noncollocated Boundary Control for Nonlinear Delayed Parabolic Dpss With Random Sensor Faults," *Journal of the Franklin Institute* 362, no. 12 (2025): 107841, https://doi.org/10.1016/j.jfranklin.2025.107841.

18. Z.-P. Wang, B.-M. Chen, J. Qiao, H.-N. Wu, and T. Huang, "Fuzzy Boundary Sampled-Data Control for Nonlinear Dpss With Random Time-Varying Delays," *IEEE Transactions on Fuzzy Systems* 32, no. 10 (2024): 5872–5885, https://doi.org/10.1109/TFUZZ.2024.3432795.

19. Z.-P. Wang, H.-N. Wu, and M. Chadli, "H Sampled-Data Fuzzy Observer Design for Nonlinear Parabolic Pde Systems," *IEEE Transactions on Fuzzy Systems* 29, no. 5 (2021): 1262–1272, https://doi.org/10.1109/TFUZZ.2020.2973943.

20. Q.-Q. Li, Z.-P. Wang, T. Huang, H.-N. Wu, H.-X. Li, and J. Qiao, "Fault-Tolerant Stochastic Sampled-Data Fuzzy Control for Nonlinear Delayed Parabolic PDE Systems," *IEEE Transactions on Fuzzy Systems* 31, no. 8 (2023): 2679–2693, https://doi.org/10.1109/tfuzz.2023.3235400.

21. X. Song, Q. Zhang, S. Song, and C. K. Ahn, "Sampled-Data-Based Event-Triggered Fuzzy Control for PDE Systems Under Cyberattacks," *IEEE Transactions on Fuzzy Systems* 30, no. 7 (2021): 2693–2705, https://doi.org/10.1109/tfuzz.2021.3092200.

22. B. Rathnayake and M. Diagne, "Observer-Based Periodic Event-Triggered and Self-Triggered Boundary Control of a Class of Parabolic PDES," *IEEE Transactions on Automatic Control* 69, no. 12 (2024): 8836–8843, https://doi.org/10.1109/TAC.2024.3419639.

23. X. Cai, K. Shi, Y. Sun, et al., "Stability Analysis of Networked Control Systems Under Dos Attacks and Security Controller Design With Mini-Batch Machine Learning Supervision," *IEEE Transactions on Information Forensics and Security* 19 (2023): 3857–3865, https://doi.org/10.1109/tifs.2023.3347889.

24. Y. Yu, W. Yang, W. Ding, and J. Zhou, "Reinforcement Learning Solution for Cyber-Physical Systems Security Against Replay Attacks," *IEEE Transactions on Information Forensics and Security* 18 (2023): 2583–2595, https://doi.org/10.1109/tifs.2023.3268532.

25. X. Cai, K. Shi, Y. Sun, et al., "Dual-Channel Ncss Performance Error Estimation Under Dos Attacks and Intelligent Control Supervised by Machine Learning to AGV Application," *IEEE Transactions on Transportation Electrification* 10, no. 3 (2023): 4882–4893, https://doi.org/10.1109/tte.2023.3328305.

26. X. Cai, Y. Sun, X. Xie, et al., "Enhancing Networked Control Systems Resilience Against Dos Attacks: A Data-Driven Approach With Adaptive Sampled-Data and Compression," *IEEE Transactions on Information Forensics and Security* 20 (2025): 4100–4109, https://doi.org/10.1109/TIFS.2025.3559464.

27. B.-M. Chen, Z.-P. Wang, F.-L. Zhao, J. Qiao, H.-N. Wu, and T. Huang, "Fault-Tolerant Event-Triggered Sampled-Data Fuzzy Control for Nonlinear Delayed Parabolic PDE Systems," *IEEE Transactions on Fuzzy Systems* 32, no. 11 (2024): 6460–6471, https://doi.org/10.1109/TFUZZ.2024.3450678.

28. S. A. Salehpour and N. M. Dehkordi, "Advanced Fault-Tolerant Control of Grid-Connected AC Microgrids Incorporating Sensor/Actuator Faults and Nonlinear Load Dynamics," *Electrical Engineering* 107, no. 8 (2025): 1–18, https://doi.org/10.1007/s00202-025-03007-9.

29. Y. Lu and W. Liu, "Disturbance Observer-Based Adaptive Fuzzy Fault-Tolerant Tracking Control for Uncertain Nonlinear Systems With Input Delay and Actuator Faults," *International Journal of Control, Automation and Systems* 21, no. 3 (2023): 820–828, https://doi.org/10.1007/s12555-021-1117-6.

30. L. Ma, Z. Wang, H. Zhang, and Q. Wang, "Adaptive Neural Network Constrained Fault Tolerant Control for Nonlinear Systems With Actuator Failures and Saturation," *IEEE Transactions on Automation Science and Engineering* (2024): 1–8, https://doi.org/10.1109/TASE.2024.3381780.

31. Z.-P. Wang, X. Zhang, J. Qiao, H.-N. Wu, and T. Huang, "Fuzzy Fault-Tolerant Boundary Control for Nonlinear DPSS With Multiple Delays and Stochastic Actuator Failures," *IEEE Transactions on Fuzzy Systems* 32, no. 5 (2024): 3121–3131, https://doi.org/10.1109/TFUZZ.2024.3367870.

32. Y.-X. Li, X. Li, B. Xu, and S. Tong, "Adaptive Actuator Failure Compensation Control of Uncertain Nonlinear PDE–ODE Cascaded Systems," *IEEE Transactions on Systems, Man, and Cybernetics: Systems* 53, no. 9 (2023): 5751–5759, https://doi.org/10.1109/tsmc.2023.3274196.

33. H. Zhang, N. Zhao, S. Wang, and R. K. Agarwal, "Improved Event-Triggered Dynamic Output Feedback Control for Networked t–s Fuzzy Systems With Actuator Failure and Deception Attacks," *IEEE Transactions on Cybernetics* 53, no. 12 (2023): 7989–7999, https://doi.org/10.1109/tcyb.2023.3264820.

34. F.-L. Zhao, Z.-P. Wang, F. Li, J. Qiao, and H.-N. Wu, "Event-Triggered Sampled–Data Fuzzy Secure Control for Nonlinear Parabolic PDE Systems Subject to Stochastic Actuator Failures and Deception Attacks," *Fuzzy Sets and Systems* 506 (2025): 109284, https://doi.org/10.1016/j.fss.2025.109284.

35. Z.-P. Wang, F.-L. Zhao, J. Qiao, H.-N. Wu, and T. Huang, "Dynamic Intermittent Boundary Control for Reaction–Diffusion Systems Under Intermittent Noncollocated Boundary Measurement," *IEEE Transactions on Systems, Man, and Cybernetics: Systems* 54, no. 5 (2024): 2884–2896, https://doi.org/10.1109/tsmc.2024.3353181.

36. S. Pasetto, M. Montejo, M. U. Zahid, et al., "Calibrating Tumor Growth and Invasion Parameters With Spectral Spatial Analysis of Cancer Biopsy Tissues," *npj Systems Biology and Applications* 10, no. 1 (2024): 112, https://doi.org/10.1038/s41540-024-00439-0.

37. J. Keener and J. Sneyd, *Mathematical Physiology: II: Systems Physiology* (Springer, 2009), https://doi.org/10.1007/978-0-387-79388-7.

38. E. P. Zemskov, M. A. Tsyganov, K. Kassner, and W. Horsthemke, "Nonlinear Waves in a Quintic Fitzhugh–Nagumo Model With Cross Diffusion: Fronts, Pulses, and Wave Trains," *Chaos: An Interdisciplinary Journal of Nonlinear Science* 31, no. 3 (2021): 033141, https://doi.org/10.1063/5.0043919.

Appendix A

Proof of Theorem 1. For $t \in [t_k, t_{k+1})$, along the solution of the fuzzy parabolic DPS Equation (9), we obtain.

$$\mathcal{L}\mathcal{V}(t) \triangleq \lim_{\sigma \to 0^+} \frac{\mathbb{E}\{\mathcal{V}(t+\sigma)|t\} - \mathcal{V}(t)}{\sigma}, \tag{A1}$$

$$\begin{aligned}\mathbb{E}\{\mathcal{LV}_1(t)\} = {} & 2\int_{\Psi}\vartheta^{\mathrm{T}}(r,t)\mathcal{Q}_1\vartheta_t(r,t)dr \\ & +2\int_{\Psi}e^{\mathrm{T}}(r,t)\mathcal{U}_a e_t(r,t)dr \\ & +\int_{\Psi}e^{\mathrm{T}}(r,t)\left(\sum_b \pi_{ab}\mathcal{U}_b\right)e(r,t)dr,\end{aligned} \tag{A2}$$

$$\begin{aligned}\mathbb{E}\{\mathcal{LV}_2(t)\} = {} & 2\int_{\Psi}\vartheta_r^{\mathrm{T}}(r,t)\mathcal{Z}_2^{\mathrm{T}}\Upsilon\vartheta_{rt}(r,t)dr \\ & +2\int_{\Psi}e_r^{\mathrm{T}}(r,t)\mathcal{U}_a^{\mathrm{T}}\Upsilon e_{rt}(r,t)dr,\end{aligned} \tag{A3}$$

$$\begin{aligned}\mathbb{E}\{\mathcal{LV}_3(t)\} = {} & 2\rho(t)\int_{\Psi}\Big\{\Big[\tilde{\vartheta}^{\mathrm{T}}(r,t)\mathcal{R}_1+\Big(\vartheta(r,t)-\tilde{\vartheta}(r,t)\Big)^{\mathrm{T}}\mathcal{R}_2\Big] \\ & \vartheta_t(r,t)+\Big[\tilde{e}^{\mathrm{T}}(r,t)\mathcal{Q}_1+(e(r,t)-\tilde{e}(r,t))^{\mathrm{T}}\mathcal{Q}_1\Big] \\ & e_t(r,t)\}dr-\int_{\Psi}\tilde{\vartheta}^{\mathrm{T}}(r,t)\mathcal{R}_1\tilde{\vartheta}(r,t)dr \\ & -\int_{\Psi}\tilde{e}^{\mathrm{T}}(r,t)\mathcal{Q}_1\tilde{e}(r,t)dr \\ & -2\int_{\Psi}\Big\{\Big[\vartheta(r,t)-\tilde{\vartheta}(r,t)\Big]^{\mathrm{T}}\mathcal{R}_2\tilde{\vartheta}(r,t) \\ & +[e(r,t)-\tilde{e}(r,t)]^{\mathrm{T}}\mathcal{Q}_2\tilde{e}(r,t)\Big\}dr,\end{aligned} \tag{A4}$$

$$\begin{aligned}\mathbb{E}\{\mathcal{LV}_4(t)\} = {} & (-2\delta)\mathcal{V}_4(t)+\rho(t)\int_{\Psi}\Big[\zeta^{\mathrm{T}}(r,t)\mathcal{M}_1\zeta(r,t) \\ & +\eta^{\mathrm{T}}(r,t)\mathcal{N}_1\eta(r,t)\Big]dr \\ & -e^{-2\delta h}\int_{\Psi}\int_{t_k}^{t}\Big[\zeta^{\mathrm{T}}(r,t)\mathcal{M}_1\zeta(r,t) \\ & +\eta^{\mathrm{T}}(r,t)\mathcal{N}_1\eta(r,t)\Big]drdt,\end{aligned} \tag{A5}$$

$$\begin{aligned}\mathbb{E}\{\mathcal{LV}_5(t)\} = {} & (-2\delta)\mathcal{V}_5(t)+\int_{\Psi}\Big[\vartheta^{\mathrm{T}}(r,t)\mathcal{J}_1\vartheta(r,t) \\ & +e^{\mathrm{T}}(r,t)\mathcal{H}_1e(r,t)\Big]dr \\ & -e^{-2\delta\overline{\tau}}\int_{\Psi}\Big[\vartheta^{\mathrm{T}}(r,t-\overline{\tau})\mathcal{J}_1\vartheta(r,t-\overline{\tau}) \\ & +e^{\mathrm{T}}(r,t-\overline{\tau})\mathcal{H}_1e\big(r,t-\overline{h}\big)\Big]dr,\end{aligned} \tag{A6}$$

$$\begin{aligned}\mathbb{E}\{\mathcal{LV}_6(t)\} = {} & (-2\delta)\mathcal{V}_6(t)+\int_{\Psi}\Big[\vartheta^{\mathrm{T}}(r,t)\mathcal{J}_2\vartheta(r,t) \\ & +e^{\mathrm{T}}(r,t)\mathcal{H}_2e(r,t)\Big]dr \\ & -e^{-2\delta\overline{\tau}}\int_{\Psi}\Big[\vartheta^{\mathrm{T}}(r,t-\tau(t))\mathcal{J}_2\vartheta(r,t-\tau(t)) \\ & +e^{\mathrm{T}}(r,t-\tau(t))\mathcal{H}_2e(r,t-\tau(t))\Big]dr,\end{aligned} \tag{A7}$$

$$\begin{aligned}\mathbb{E}\{\mathcal{LV}_7(t)\} = {} & (-2\delta)\mathcal{V}_7(t)+\overline{\tau}^2\int_{\Psi}\Big[\vartheta_t^{\mathrm{T}}(r,t)\mathcal{J}_3\vartheta_t(r,t) \\ & +e_t^{\mathrm{T}}(r,t)\mathcal{H}_3e_t(r,t)\Big]dr \\ & -\overline{\tau}e^{-2\delta\overline{\tau}}\int_{\Psi}\int_{t-\overline{\tau}}^{t}\Big[\vartheta_{\varphi}^{\mathrm{T}}(r,\varphi)\mathcal{J}_3\vartheta_{\varphi}(r,\varphi) \\ & +e_{\varphi}^{\mathrm{T}}(r,\varphi)\mathcal{H}_3e_{\varphi}(r,\varphi)\Big]d\varphi dr.\end{aligned} \tag{A8}$$

Applying Lemma 2 [27] to Equation (A8), it can be obtained

$$\begin{aligned} & -\overline{\tau}e^{-2\delta\overline{\tau}}\int_{\Psi}\int_{t-\overline{\tau}}^{t}\vartheta_{\varphi}^{\mathrm{T}}(r,\varphi)\,\mathcal{J}_3\vartheta_{\varphi}(r,\varphi)d\varphi dr \\ = {} & -\overline{\tau}e^{-2\delta\overline{\tau}}\int_{\Psi}\int_{t-\overline{\tau}}^{t-\tau(t)}\vartheta_{\varphi}^{\mathrm{T}}(r,\varphi)\,\mathcal{J}_3\vartheta_{\varphi}(r,\varphi)d\varphi \\ & -\overline{\tau}e^{-2\delta\overline{\tau}}\int_{\Psi}\int_{t-\tau(t)}^{t}\vartheta_{\varphi}^{\mathrm{T}}(r,\varphi)\,\mathcal{J}_3\vartheta_{\varphi}(r,\varphi)d\varphi \\ \leqslant {} & -e^{-2\delta\overline{\tau}}\int_{\Psi}[\vartheta(r,t)-\vartheta(r,t-\tau(t))]^{\mathrm{T}}\mathcal{J}_3 \\ & [\vartheta(r,t)-\vartheta(r,t-\tau(t))]dr.\end{aligned} \tag{A9}$$

Select $\psi(r,t) = \mathrm{col}\{\vartheta(r,t),\ \vartheta(r,t_k),\ \vartheta_r(r,t),\ \vartheta_t(r,t),\ \vartheta(r,t-\tau(t)),\ \vartheta(r,t-\overline{\tau}),\ \vartheta(l_2,t),\ \vartheta(l_2,t_k),\ \vartheta_t(l_2,t)\}$, $\tilde{\vartheta}(r,t) = \vartheta(r,t)-\vartheta(r,t_k) = \int_{t-r(t)}^{t}\vartheta_{\theta}(r,t)\mathrm{d}\theta$, $r(t) = t-t_k$ and $\rho(t) = t_{k+1}-t$. Then, for any matrices $\mathcal{U}\in\mathbb{R}^{9n_{\vartheta}\times n_{\vartheta}}$, we can gives the following relationship:

$$\begin{aligned}0 = {} & 2\int_{\Psi}\sum_{i=1}^{m}\sum_{j=1}^{m}\sum_{z=1}^{m}\mathcal{W}_i(\delta(r,t))\mathcal{W}_j\Big(\hat{\delta}(l_1,t_k)\Big)\mathcal{W}_z\Big(\hat{\delta}(l_2,t_k)\Big) \\ & \times\psi^{\mathrm{T}}(r,t)\mathcal{U}\Big\{\tilde{\vartheta}(r,t)-\int_{t_k}^{t}\vartheta_{\theta}(r,\theta)d\theta\Big\}dr.\end{aligned} \tag{A10}$$

Consider $P = \left[\mathcal{P}\ 0_{n_z\times n_z}\ \mathcal{Z}_2\ 0_{n_{\vartheta}\times 5n_{\vartheta}}\right]^{\mathrm{T}}\in\mathbb{R}^{8n_z\times n_{\vartheta}}$. Using Equation (17), the following relationship is given:

$$\begin{aligned}0 = {} & 2\mathbb{E}\Big\{\int_{\Psi}\big(\vartheta^{\mathrm{T}}(s,t)\mathcal{P}^{\mathrm{T}}+\vartheta_t^{\mathrm{T}}(s,t)\mathcal{Z}_2^{\mathrm{T}}\big) \\ & \Big[\{\Upsilon\vartheta_r(r,t)\}_r+\sum_{i=1}^{m}\mathcal{W}_i(\delta(r,t))\{A_i r(s,t) \\ & +A_{di}\vartheta(r,t-\tau(t))-\vartheta_t(r,t)\}dr\Big\}.\end{aligned} \tag{A11}$$

Integration Equation (A11) yields, we can obtain

$$\begin{aligned} & 2\int_{\Psi}(\vartheta^{\mathrm{T}}(r,t)\mathcal{P}^{\mathrm{T}}+\vartheta_t^{\mathrm{T}}(r,t)\mathcal{Z}_2^{\mathrm{T}})\{\Upsilon\vartheta_r(r,t)\}_r dr \\ = {} & 2\big(\vartheta^{\mathrm{T}}(r,t)\mathcal{P}^{\mathrm{T}}+\vartheta_t^{\mathrm{T}}(r,t)\mathcal{Z}_2^{\mathrm{T}}\big)\Upsilon\vartheta_r(r,t)|_{l_1}^{l_2} \\ & -2\int_{\Psi}(\vartheta_r^{\mathrm{T}}(r,t)\mathcal{P}^{\mathrm{T}}+\vartheta_{tr}^{\mathrm{T}}(r,t)\mathcal{Z}_2^{\mathrm{T}})\Upsilon\vartheta_r(r,t)dr \\ = {} & 2\vartheta^{\mathrm{T}}(l_2,t)\mathcal{P}^{\mathrm{T}}\Upsilon\vartheta_r(l_2,t)+2\vartheta_t^{\mathrm{T}}(r,t)\mathcal{Z}_2^{\mathrm{T}}\Upsilon\vartheta_r(l_2,t) \\ & -2\int_{\Psi}\vartheta_r^{\mathrm{T}}(r,t)\mathcal{P}^{\mathrm{T}}\Upsilon\vartheta_r(r,t)dr \\ & -2\int_{\Psi}\vartheta_{tr}^{\mathrm{T}}(r,t)\mathcal{Z}_2^{\mathrm{T}}\Upsilon\vartheta_r(r,t)dr \\ = {} & 2\sum_{z=1}^{m}\mathcal{W}_z\Big(\hat{\delta}(l_2,t_k)\Big)\vartheta^{\mathrm{T}}(l_2,t)\mathcal{P}^{\mathrm{T}}\Upsilon\mathcal{B}\mathcal{K}_z \\ & \Big[(1-\alpha)(1-\beta)\hat{\vartheta}(l_2,t_k)+\alpha(1-\beta)f\Big(\hat{\vartheta}(l_2,t_k)\Big)\Big] \\ & +2\sum_{z=1}^{m}\mathcal{W}_z\Big(\hat{\delta}(l_2,t_k)\Big)\vartheta_t^{\mathrm{T}}(r,t)\mathcal{Z}_2^{\mathrm{T}}\Upsilon\mathcal{D}_q\mathcal{B}\mathcal{K}_z \\ & \Big[(1-\alpha)(1-\beta)\hat{\vartheta}(l_2,t_k)+\alpha(1-\beta)f\Big(\hat{\vartheta}(l_2,t_k)\Big)\Big] \\ & -\int_{\Psi}\vartheta_r^{\mathrm{T}}(r,t)\{\mathcal{P}^{\mathrm{T}}\Upsilon+\Upsilon\mathcal{P}\}\vartheta_r(r,t)dr \\ & -2\int_{\Psi}\vartheta_{tr}^{\mathrm{T}}(r,t)\mathcal{Z}_2^{\mathrm{T}}\Upsilon\vartheta_r(r,t)dr,\end{aligned} \tag{A12}$$

in which $\hat{\vartheta}(l_2,t_k) = \vartheta(l_2,t_k)-e(l_2,t_k)$.

According to Lemma 1 [17], the relationship can be determined as follows:

$$
\begin{aligned}
&- \int_{\Psi} \vartheta_r^{\mathrm{T}}(r,t)\{\mathcal{P}^{\mathrm{T}}\Upsilon + \Upsilon\mathcal{P}\}\vartheta_r(r,t)dr \\
&\leqslant -\int_{\Psi} \vartheta_r^{\mathrm{T}}(r,t)\{\mathcal{P}^{\mathrm{T}}\Upsilon + \Upsilon\mathcal{P} - \mathcal{U}\}\vartheta_r(r,t)dr \\
&\quad - \frac{\pi^2}{4(l_2-l_1)^2}\int_{\Psi}\{\vartheta(r,t)-\vartheta(l_2,t)\}^{\mathrm{T}}\mathcal{U} \\
&\quad \{\vartheta(r,t)-\vartheta(l_2,t)\}dr.
\end{aligned} \tag{A13}
$$

From Equation (19), there exists a symmetric matrix E satisfying the following inequality:

$$
0 \leq \hat{h}_{l_2}^{\mathrm{T}}(t_k)C^{\mathrm{T}}EC\hat{h}_{l_2}(t_k) - f^{\mathrm{T}}\left(\hat{h}_{l_2}(t_k)\right)Ef\left(\hat{h}_{l_2}(t_k)\right). \tag{A14}
$$

Using Equations (A1–A13), one obtains

$$
\begin{aligned}
&\mathbb{E}\{\mathcal{L}\mathcal{V}_\vartheta(t) + 2\delta\mathcal{V}_\vartheta(t)\}\} \\
&\leq \sum_{i=1}^{m}\sum_{j=1}^{m}\sum_{z=1}^{m}\mathcal{W}_i(\delta(r,t))\mathcal{W}_j\left(\hat{\delta}(l_1,t_k)\right)\mathcal{W}_z\left(\hat{\delta}(l_2,t_k)\right) \\
&\int\Bigg\{\psi^{\mathrm{T}}(r,t)T_{1\vartheta ij}(m_k)\psi(r,t) \\
&-\int_{t_k}^{t}\begin{bmatrix}\psi(r,t)\\ f\left(\hat{h}_{l_2}(t_k)\right)\\ \vartheta_v(r,v)\end{bmatrix}^{\mathrm{T}}T_{3f,\vartheta ij}\begin{bmatrix}\psi(r,t)\\ f\left(\hat{h}_{l_2}(t_k)\right)\\ \vartheta_v(r,v)\end{bmatrix}\Bigg\}dvdr \\
&-2\sum_{z=1}^{m}\mathcal{W}_z\left(\hat{\delta}(l_2,t_k)\right)\vartheta^{\mathrm{T}}(l_2,t)\mathcal{P}^{\mathrm{T}}\Upsilon\mathcal{B}\mathcal{K}_z(1-\alpha)(1-\beta)e(l_2,t_k) \\
&-2\sum_{z=1}^{m}\mathcal{W}_z\left(\hat{\delta}(l_2,t_k)\right)\vartheta_t^{\mathrm{T}}(l_2,t)\mathcal{Z}_2^{\mathrm{T}}\Upsilon\mathcal{D}_q\mathcal{B}\mathcal{K}_z\alpha(1-\beta)e(l_2,t_k).
\end{aligned} \tag{A15}
$$

The process of proving the error system $e(r,t)$ follows in the same way:

$$
\begin{aligned}
&\mathbb{E}\{\mathcal{L}\mathcal{V}_e(t) + 2\delta\mathcal{V}_e(t)\}\} \\
&\leq \sum_{i=1}^{m}\sum_{j=1}^{m}\sum_{z=1}^{m}\mathcal{W}_i(\delta(r,t))\mathcal{W}_j\left(\hat{\delta}(l_1,t_k)\right)\mathcal{W}_z\left(\hat{\delta}(l_2,t_k)\right) \\
&\int\Bigg\{\varepsilon^{\mathrm{T}}(r,t)T_{1a,eij}(m_k)\varepsilon(r,t) \\
&-\int_{t_k}^{t}\begin{bmatrix}\varepsilon(r,t)\\ e_v(r,v)\end{bmatrix}^{\mathrm{T}}T_{3eij}\begin{bmatrix}\varepsilon(r,t)\\ e_v(r,v)\end{bmatrix}\Bigg\}dvdr.
\end{aligned} \tag{A16}
$$

Connect Equations (A15) and (A16) and (20), we can obtain:

$$
\begin{aligned}
&\mathbb{E}\{\mathcal{L}\mathcal{V}(t) + 2\delta\mathcal{V}(t)\}\} \\
&+\int_{\Psi}\overline{\vartheta}(r,t)^{\mathrm{T}}\overline{\mathcal{O}}\overline{\vartheta}(r,t)dr - \gamma^2\int_{\Psi}\overline{\omega}(r,t)^{\mathrm{T}}\overline{\omega}(r,t)dr \\
&\leq \sum_{i=1}^{m}\sum_{j=1}^{m}\sum_{z=1}^{m}\mathcal{W}_i(\delta(r,t))\mathcal{W}_j\left(\hat{\delta}(l_1,t_k)\right)\mathcal{W}_z\left(\hat{\delta}(l_2,t_k)\right) \\
&\quad\int_{\Psi}\Big\{\overline{\Phi}^{\mathrm{T}}(r,t)T_{1\vartheta eij} + \rho(t)T_{2\vartheta e}\overline{\Phi}(r,t) \\
&\quad -\int_{t_k}^{t}\overline{\theta}(r,t)^{\mathrm{T}}T_{3f,\vartheta e}\overline{\theta}(r,t)dvdr \\
&\quad = \int_{\Psi}\Bigg\{\frac{\rho(t)}{h_k}\overline{\Phi}^{\mathrm{T}}(r,t)\Phi_{1\vartheta eij}(m_k)\overline{\Phi}(r,t) \\
&\quad +\int_{t_k}^{t}\overline{\theta}(r,t)^{\mathrm{T}}\Phi_{2a,\vartheta eij}(m_k)\overline{\theta}(r,t)\Bigg\}dv,
\end{aligned} \tag{A17}
$$

where $\overline{\Phi}(r,t) = \mathrm{col}\{\psi(r,t), \varepsilon(r,t), \overline{\omega}(r,t)\}$, $\overline{\theta}(r,t) = \mathrm{col}\{\overline{\Phi}(r,t), f(\hat{y}_{l_2}(t_k)), \vartheta_v(r,v), e_v(r,v)\}$, $\Phi_{1a,\vartheta eij}(m_k) = T_{1\vartheta eij} + m_k T_{2\vartheta e}$, $\Phi_{2a,\vartheta eij}(m_k) = \begin{bmatrix} T_{1a,\vartheta eij} & 0*0\end{bmatrix} - m_k$.

Clearly, if the subsequent inequality tests are satisfied:

$$
\begin{aligned}
&\sum_{i=1}^{m}\sum_{j=1}^{m}\sum_{z=1}^{m}\mathcal{W}_i(\delta(r,t))\mathcal{W}_j\left(\hat{\delta}(l_1,t_k)\right)\mathcal{W}_z\left(\hat{\delta}(l_2,t_k)\right)\Phi_{ra,\vartheta eij}(m_k) \\
&< 0, r = 1, 2.
\end{aligned} \tag{A18}
$$

Furthermore, we have

$$
\begin{aligned}
&\mathbb{E}\{\mathcal{L}\mathcal{V}(t) + 2\delta\mathcal{V}(t)\}\} \\
&+\int_{\Psi}\overline{\vartheta}(r,t)^{\mathrm{T}}\overline{\mathcal{O}}\,\overline{\vartheta}(r,t)dr - \gamma^2\int_{\Psi}\overline{\omega}(r,t)^{\mathrm{T}}\overline{\omega}(r,t)dr \leq 0.
\end{aligned} \tag{A19}
$$

Form Equation (A19), it can be transformed into

$$
\begin{aligned}
&\int_{\Psi}\overline{\vartheta}(r,t)^{\mathrm{T}}\overline{\mathcal{O}}\,\overline{\vartheta}(r,t)dr \\
&\leq -\mathbb{E}\{\mathcal{L}\mathcal{V}(t) + 2\delta\mathcal{V}(t)\} + \gamma^2\int_{\Psi}\overline{\omega}(r,t)^{\mathrm{T}}\overline{\omega}(r,t)dr\Bigg\}\Bigg\}.
\end{aligned} \tag{A20}
$$

Subsequently, combining the aforementioned inequality

$$
\begin{aligned}
&\int_{t_0}^{t_f}\int_{\Psi}\overline{\vartheta}(r,t)^{\mathrm{T}}\overline{\mathcal{O}}\overline{\vartheta}(r,t)drdt \\
&\leq \mathcal{V}(t_0) - \mathcal{V}(t_f) + \gamma^2\int_{t_0}^{t_f}\int_{\Psi}\overline{\omega}(r,t)^{\mathrm{T}}\overline{\omega}(r,t)drdt \\
&\leq \mathcal{V}(t_0) + \gamma^2\int_{t_0}^{t_f}\int_{\Psi}\overline{\omega}(r,t)^{\mathrm{T}}\overline{\omega}(r,t)drdt.
\end{aligned} \tag{A21}
$$

This implies that the H_∞ performance in Equation (20) satisfies the prescribed attenuation level γ.

From Equation (27), we obtain

$$
\Phi_{ra,\vartheta eij}(m) < 0, r = 1, 2, \tag{A22}
$$

and

$$
\Phi_{ra,\vartheta eij}(\varepsilon) < 0, r = 1, 2, \tag{A23}
$$

$$
\begin{aligned}
\Phi_{ra,\vartheta eij}(m_k) &= \frac{m-m_k}{m-\varepsilon}\Phi_{ra,\vartheta eij}(\varepsilon) \\
&\quad + \frac{m_k-\varepsilon}{m-\varepsilon}\Phi_{ra,\vartheta eij}(m) < 0.
\end{aligned} \tag{A24}
$$

Then, it follows from Equation (A19), one obtains

$$
\begin{aligned}
V(t) &< V(t_k)\mathrm{e}^{-2\alpha(t-t_k)} < V(t_k^-)\mathrm{e}^{-2\delta(t-t_k)} \\
&< V(t_{k-1})\mathrm{e}^{-2\delta(t-t_{k-1})} \\
&< \ldots \\
&< V(t_0)\mathrm{e}^{-2\delta(t-t_0)}.
\end{aligned} \tag{A25}
$$

Therefore, from Equation (A25), we can obtain that fuzzy delayed DPSs Equation (17) is mean square exponentially stable.

The following is a summary of the symbols used in the paper, along with detailed definitions and explanations of their meanings.

$$Y_1 = e_1 - e_2, Y_2 = e_5 - e_6, Y_3 = e_1 - e_5, Y_4 = e_1 - e_7,$$
$$Y_5 = e_{10} - e_{11} Y_6 = e_{14} - e_{15}, Y_7 = e_{10} - e_{15}, Y_8 = e_{10} - e_{16},$$
$$\Omega_1 = \mathrm{Sym}\{e_1^{\mathrm{T}} \mathcal{Z}_1 e_4\}, \omega_2 = \mathrm{Sym}\{e_2^{\mathrm{T}} \mathcal{R}_2 Y_1\},$$
$$\Omega_3 = \mathrm{Sym}\{e_7^{\mathrm{T}} \mathcal{P}^{\mathrm{T}} \Upsilon \mathcal{D}_q \mathcal{B} \mathcal{K}_z e_8\}, \Omega_4 = \mathrm{Sym}\{e_4^{\mathrm{T}} \mathcal{Z}_2^{\mathrm{T}} \Upsilon \mathcal{D}_q \mathcal{B} \mathcal{K}_z e_8\},$$
$$\Omega_5 = \mathrm{Sym}\{e_1^{\mathrm{T}} \mathcal{P}^{\mathrm{T}} e_4\}, \Omega_6 = \mathrm{Sym}\{\mathcal{U} Y_1\}, \omega_7 = \mathrm{Sym}\{e_{10}^{\mathrm{T}} \mathcal{U}_a e_{13}\},$$
$$\Omega_8 = \mathrm{Sym}\{e_{11}^{\mathrm{T}} \mathcal{Q}_2 Y_5\}, \Omega_9 = \mathrm{Sym}\{e_{16}^{\mathrm{T}} \mathcal{S}^{\mathrm{T}} \Upsilon \mathcal{L}_j e_{17}\},$$
$$\Omega_{10} = \mathrm{Sym}\{e_{19}^{\mathrm{T}} \mathcal{U}_2^{\mathrm{T}} \Upsilon \mathcal{L}_j e_{17}\}, \Omega_{11} = \mathrm{Sym}\{e_{10}^{\mathrm{T}} \mathcal{S}^{\mathrm{T}} \mathcal{I}_j e_{17}\},$$
$$\Omega_{12} = \mathrm{Sym}\{e_{10}^{\mathrm{T}} \mathcal{S}^{\mathrm{T}} e_{13}\}, \Omega_{13} = \mathrm{Sym}\{e_{13}^{\mathrm{T}} \mathcal{U}_2^{\mathrm{T}} \mathcal{I}_j e_{17}\},$$
$$\Omega_{14} = \mathrm{Sym}\{\mathcal{H} Y_5\}, \Omega_{15} = \mathrm{Sym}\{Y_1^{\mathrm{T}} \mathcal{R}_1 e_4\}, \omega_{16} = \mathrm{Sym}\{e_2^{\mathrm{T}} \mathcal{R}_2 e_4\},$$
$$\Omega_{17} = \mathrm{Sym}\{e_2^{\mathrm{T}} \mathcal{R}_2 Y_1\}, \Omega_{18} = \mathrm{Sym}\{e_4^{\mathrm{T}} \mathcal{M}_{12} e_2\},$$
$$\Omega_{19} = \mathrm{Sym}\{Y_5^{\mathrm{T}} \mathcal{Q}_1 e_{13}\}, \Omega_{20} = \mathrm{Sym}\{e_{11}^{\mathrm{T}} \mathcal{Q}_2 e_{13}\},$$
$$\Omega_{21} = \mathrm{Sym}\{e_{13}^{\mathrm{T}} \mathcal{N}_{12} e_{11}\},$$
$$\omega_1 = \mathrm{Sym}\{\mathcal{P}^{\mathrm{T}} \Upsilon\}, \omega_2 = \mathrm{Sym}\{\mathcal{P}^{\mathrm{T}} \mathcal{A}_i\}, \omega_3 = \mathrm{Sym}\{\mathcal{P}^{\mathrm{T}} \mathcal{A}_{di}\},$$
$$\omega_4 = \mathrm{Sym}\{\mathcal{Z}_2^{\mathrm{T}} \mathcal{A}_i\}, \omega_5 = \mathrm{Sym}\{\mathcal{Z}_2^{\mathrm{T}} \mathcal{A}_{di}\}, \omega_6 = \mathrm{Sym}\{\mathcal{Z}_2^{\mathrm{T}}\},$$
$$\omega_7 = \mathrm{Sym}\{\mathcal{U}_2^{\mathrm{T}} \Upsilon\}, \omega_8 = \mathrm{Sym}\{\mathcal{S}^{\mathrm{T}} \Upsilon\}, \omega_9 = \mathrm{Sym}\{\mathcal{S}^{\mathrm{T}} \mathcal{A}_i\},$$
$$\omega_{10} = \mathrm{Sym}\{\mathcal{S}^{\mathrm{T}} \mathcal{A}_{dj}\}, \omega_{11} = \mathrm{Sym}\{\mathcal{U}_2^{\mathrm{T}} \mathcal{A}_j\},$$
$$\omega_{12} = \mathrm{Sym}\{\mathcal{U}_2^{\mathrm{T}} \mathcal{A}_{dj}\}, \omega_{13} = \mathrm{Sym}\{\mathcal{U}_2^{\mathrm{T}}\},$$
$$\Pi_1 = \mathrm{col}\{\zeta_1, 2\delta \mathcal{Z}_1, \mathcal{J}_1, \mathcal{J}_2, \omega_6\}, \Pi_2 = \mathrm{col}\{\zeta_2, \overline{h}^2 \mathcal{J}_3, \omega_6\},$$
$$\Pi_3 = \mathrm{col}\{2\delta \mathcal{Z}^{\mathrm{T}} \Upsilon, \omega_5 - \mathcal{D}\}, \Pi_4 = \mathrm{col}\{Y_2, Y_3\},$$
$$\Pi_5 = \mathrm{col}\left\{\sum_{b=1} \pi_{ab} \mathcal{U}_b, 2\delta \mathcal{U}_a, \mathcal{H}_1, \mathcal{H}_2, \omega_9\right\},$$
$$\Pi_6 = \mathrm{col}\{\delta\omega_7, -\omega_8, -(\omega_8 - \mathcal{K})\}, \Pi_7 = \mathrm{col}\{Y_6, Y_7\},$$
$$\wedge_1 = (l_2 - l_1)(1 - \alpha)(1 - \beta),$$
$$\overline{\Omega}_1 = \mathrm{Sym}\{e_1^{\mathrm{T}} \overline{\mathcal{Z}}_1 e_4\}, \overline{\Omega}_2 = \mathrm{Sym}\{e_2^{\mathrm{T}} \overline{\mathcal{R}}_2 Y_1\},$$
$$\overline{\Omega}_3 = \mathrm{Sym}\{e_7^{\mathrm{T}} \Upsilon \mathcal{D}_q \mathcal{B} \overline{\mathcal{K}}_z e_8\}, \overline{\Omega}_4 = \mathrm{Sym}\{e_4^{\mathrm{T}} \Upsilon \mathcal{D}_q \mathcal{B} \overline{\mathcal{K}}_z e_8\},$$
$$\overline{\Omega}_5 = \mathrm{Sym}\{e_1^{\mathrm{T}} \mathcal{V} e_4\}, \overline{\Omega}_6 = \mathrm{Sym}\{\overline{\mathcal{U}} Y_1\}, \overline{\Omega}_7 = \mathrm{Sym}\{e_{10}^{\mathrm{T}} \overline{\mathcal{U}}_a e_{13}\},$$
$$\overline{\Omega}_8 = \mathrm{Sym}\{e_{11}^{\mathrm{T}} \overline{\mathcal{Q}}_2 Y_5\}, \overline{\Omega}_9 = \mathrm{Sym}\{e_{16}^{\mathrm{T}} \Upsilon \overline{\mathcal{L}}_j e_{17}\},$$
$$\overline{\Omega}_{10} = \mathrm{Sym}\{e_{19}^{\mathrm{T}} \Upsilon \overline{\mathcal{L}}_j e_{17}\}, \overline{\Omega}_{11} = \mathrm{Sym}\{e_{10}^{\mathrm{T}} \overline{\mathcal{I}}_j e_{17}\},$$
$$\overline{\Omega}_{12} = \mathrm{Sym}\{e_{10}^{\mathrm{T}} \overline{\mathcal{V}}^{\mathrm{T}} e_{13}\}, \overline{\Omega}_{13} = \mathrm{Sym}\{e_{13}^{\mathrm{T}} \overline{\mathcal{I}}_j e_{17}\},$$
$$\overline{\Omega}_{14} = \mathrm{Sym}\{\overline{\mathcal{H}} Y_5\}, \overline{\Omega}_{15} = \mathrm{Sym}\{Y_1^{\mathrm{T}} \overline{\mathcal{R}}_1 e_4\},$$
$$\overline{\Omega}_{16} = \mathrm{Sym}\{e_2^{\mathrm{T}} \overline{\mathcal{R}}_2 e_4\}, \overline{\Omega}_{17} = \mathrm{Sym}\{e_2^{\mathrm{T}} \overline{\mathcal{R}}_2 Y_1\},$$
$$\overline{\Omega}_{18} = \mathrm{Sym}\{e_4^{\mathrm{T}} \overline{\mathcal{M}}_{12} e_2\}, \overline{\Omega}_{19} = \mathrm{Sym}\{Y_5^{\mathrm{T}} \overline{\mathcal{Q}}_1 e_{13}\},$$
$$\overline{\Omega}_{20} = \mathrm{Sym}\{e_{11}^{\mathrm{T}} \overline{\mathcal{Q}}_2 e_{13}\}, \overline{\Omega}_{21} = \mathrm{Sym}\{e_{13}^{\mathrm{T}} \overline{\mathcal{N}}_{12} e_{11}\},$$
$$\overline{\omega}_1 = \mathrm{Sym}\{\Upsilon \overline{\mathcal{V}}\}, \overline{\omega}_2 = \mathrm{Sym}\{\mathcal{A}_i \overline{\mathcal{V}}\}, \overline{\omega}_3 = \mathrm{Sym}\{\mathcal{A}_{di} \overline{\mathcal{V}}\},$$
$$\overline{\omega}_4 = \mathrm{Sym}\{\overline{\mathcal{V}}^{\mathrm{T}}\}, \overline{\omega}_5 = \mathrm{Sym}\{\mathcal{A}_j \overline{\mathcal{V}}\}, \overline{\omega}_6 = \mathrm{Sym}\{\mathcal{A}_{dj} \overline{\mathcal{V}}\},$$
$$\overline{\Pi}_1 = \mathrm{col}\left\{\overline{\zeta}_1, 2\delta \overline{\mathcal{Z}}_1, \overline{\mathcal{J}}_1, \overline{\mathcal{J}}_2, d_1 \overline{\omega_2}, \mathcal{O}_1\right\},$$
$$\overline{\Pi}_2 = \mathrm{col}\left\{\overline{\zeta}_2, \overline{h}^2 \overline{\mathcal{J}}_3, r_1 \overline{\omega_4}\right\}, \overline{\Pi}_3 = \mathrm{col}\{\delta r_1 \overline{\omega_1}, d_1 \overline{\omega_1} - \overline{\mathcal{D}}\},$$
$$\overline{\Pi}_5 = \mathrm{col}\left\{\sum_{b=1} \pi_{ab} \overline{\mathcal{U}}_b, 2\delta \overline{\mathcal{U}}_a, \overline{\mathcal{H}}_1, \overline{\mathcal{H}}_2, \overline{\omega}_5\right\},$$
$$\overline{\Pi}_6 = \mathrm{col}\{\delta r_2 \overline{\omega}_1, d_2 \overline{\omega}_1, d_2 \overline{\omega}_1 - \mathcal{K})\},$$
$$\overline{\Pi}_7 = \mathrm{col}\{\mathcal{F}_i \mathcal{A}_i \overline{\mathcal{V}}, -\mathcal{F}_i \mathcal{A}_{di}\}, \overline{\Pi}_8 = \mathrm{col}\{\mathcal{A}_i, -\mathcal{A}_{di}\},$$
$$\overline{\Pi}_9^{\mathrm{T}} = \mathrm{col}\{e_1^{\mathrm{T}}, e_4^{\mathrm{T}}, e_{10}^{\mathrm{T}}.e_{13}^{\mathrm{T}}\},$$
$$\wedge_2 = \varpi(\overline{\mathcal{V}} + \overline{\mathcal{V}}^{\mathrm{T}}) - \varpi^2 I.$$